THESIS FOR THE DEGREE OF LICENTIATE OF ENGINEERING

Molten Salt Electrolytes for Calcium Batteries

JOHANNA TIMHAGEN

Department of Physics

CHALMERS UNIVERSITY OF TECHNOLOGY

Gothenburg, Sweden 2023

Molten Salt Electrolytes for Calcium Batteries
JOHANNA TIMHAGEN

Department of Physics
Chalmers University of Technology
SE-412 96 Gothenburg
Sweden
Telephone + 46 (0)31-772 1000

Cover:
Abstract illustration of cations.

Printed by Chalmers Reproservice
Gothenburg, Sweden 2023

Molten Salt Electrolytes for Calcium Batteries

Johanna Timhagen
Department of Physics
Chalmers University of Technology

Abstract

Batteries are in higher demand than ever before as well as increased requirements in terms of energy and power density. The desire for higher energy density has meant that electrolytes are pushed above their electrochemical stability limits and hence they decompose, but typically this is under control and a new beneficial phase is created at the electrode surface; the solid electrolyte interphase (SEI).

Here calcium batteries (CaBs) are targeted. The large abundance of Ca in the Earth's crust and its relatively low electrochemical potential make CaBs a very attractive alternative. However, Ca metal anodes commonly experience issues with ion-isolating phases, associated with organic electrolytes and in particular their solvents, which turn the SEIs from favorable to detrimental. Herein, we create completely solvent-free electrolytes in the form of molten salt electrolytes (MSEs), i.e. binary and multi-component systems of inorganic cations and anions, whereby this issue potentially can be avoided.

For all studies herein, studying thermal properties has been crucial, both to better understand the compositional entropy effect of MSEs, which is shown to reduce the melting temperature from >100 °C to 55-75 °C, and as input to a predictive model for the solubility of possible SEI components, including those for CaBs. Future work based on these findings includes refined MSEs and detailed studies of electrochemical properties of MSEs for/in CaBs, as well as CaB full-cell tests.

Keywords: Molten salt electrolytes, Calcium, Metal anodes

List of Papers

This thesis is based on the work contained in the following papers:

I **Local structure and cation coordination in multi-cationic molten salt electrolytes.**
J. Timhagen, C. C. Cardona, Jonathan Weidow and P. Johansson
Manuscript.

II **"A proposal of a modelling route to predict the solubility of solid electrolyte interphase (SEI) species",**
J. Timhagen, V. Thangavel, Jonathan Weidow and P. Johansson
Manuscript.

Contribution Report

I JT prepered the molten salt electrolytes and performed TGA, DSC and Raman spectroscopy measurements. JT wrote the first draft of the manuscript

II JT performed the DSC experiments, wrote corresponding parts of the manuscript and participated in the revision of the full manuscript.

Table of Contents

List of Abbreviations

CaB	Calcium Battery
CEI	Cathode Electrolyte Interphase
COSMO-RS	Conductor-like Screening Model for Real Solvents
DFT	Density Functional Theory
DSC	Differential Scanning Calorimetry
ESW	Electrochemical Stability Window
EV	Electric Vehicle
HEA	High Entropy Alloy
HEE	High Entropy Electrolyte
HCE	Highly Concentrated Electrolyte
HOMO	Highest Occupied Molecular Orbital
IL	Ionic Liquid
LIB	Lithium-Ion Battery
LUMO	Lowest Unoccupied Molecular Orbital
MS	Molten Salt
MSE	Molten Salt Electrolyte
SEI	Solid Electrolyte Interphase
SHE	Standard Hydrogen Electrode
RDS	Rate Determining Step
TGA	Thermal Gravimetric Analysis

Chapter 1

Introduction

The success of the lithium-ion battery (LIB) has led to power sources for mobile phones, power tools, and electric vehicles (EVs), to mention a few [1]. Still, batteries increasingly find their way into new applications and thus creating new demands. Additionally, the appliances batteries are already present in, particularly EVs, are in higher demand than ever, which leads to increased requirements on batteries in terms of cost, energy and power density, safety, and life length [2]. Consequently, finding new battery technologies is a worldwide research quest.

A new/old concept is metal anodes, which in contrast to the LIB chemistry which is realised through intercalation anodes [3], has been deemed far too unsafe. The safety issues largely come from the use of lithium metal, which is very prone to dendritic growth and is one common underlying cause of short-circuiting [4]. Still, enabling the use of metallic anodes in batteries would lead to higher energy densities. Three elements that in principle are very attractive metal anodes are Al, Ca, and Mg, which are the 3rd, 5th, and 7th most abundant elements in the Earth's crust, respectively [5]. Al, Ca, and Mg have also been shown to be less prone to dendritic growth [6], and in addition, these three elements are multivalent, which means that 2 or 3 e^- are transported for every cation.

Calcium batteries (CaBs) are still in their infancy [7], which largely comes from the reactivity of the Ca metal surface, which is exceptionally prone to oxidation [8]. In fact, until rather recently [9], stable plating and stripping of Ca metal anodes and hence rechargeability of CaBs was deemed impossible, due to these stable phases formed at the electrolyte/electrode interface, completely blocking Ca^{2+} transfer [8]. Since the pivotal breakthrough, CaBs have attracted more interest, but new battery designs – such as using novel electrolyte concepts – are needed to achieve stable cycling of Ca metal anodes, preferably at room temperature. This leads to the first important concept of this thesis; designing new electrolytes for CaBs.

The design concept that is explored in this thesis is molten salt electrolytes (MSEs), i.e. binary and multi-component systems of inorganic cations and anions. These are completely solvent-free, hence, avoiding issues associated with organic solvents, such as the blocking of Ca^{2+} transfer and electrolyte flammability [8], and they do not induce a high polarization, as opposed to when using ionic liquid-based electrolytes [10]. In particular, we have used the calcium bis(fluorosulfonyl)imide ($Ca(FSI)_2$) salt together with analogous Li-, Na-, and KFSI salts and studied them both separately and in equimolar ternary and quaternary compositions, all to explore the physicochemical electrolyte properties as functions of the compositional entropy.

The second important concept in this thesis looks at the possibility of predicting the solubility of SEI components/salt in common electrolytes. The model was first built and validated for LIB electrolytes by comparing it to experimental data. Thereafter, Na-, Ca- and Mg-containing electrolytes were modelled. Herein, the thermal properties of the SEI-species together with their solubility in water are discussed, with particular emphasis on the divalent ions.

For all studies herein, studying thermal properties has been crucial. The focus lay on a better understanding of electrolyte properties; both when the compositional entropy is increased in solvent-free electrolytes, but also on how the solubility of divalent cations behave in solutions. Background on the electrochemical properties of electrolytes is presented to put these electrolytes in their context, but experimental data on such properties is out of the scope of this thesis. Future work based on these findings includes refined MSEs and detailed studies of electrochemical properties of MSEs for/in CaBs, as well as CaB full-cell tests.

Chapter 2

Batteries

A lot has happened since the first battery, the "Voltaic pile", was invented by Alessandro Volta in 1799. The pile was part copper and part zinc with salt water as an electrolyte [11], [12]. All batteries the following 100 years were primary batteries, intended to be used once and then thrown away. It was not until Waldemar Jungner created the nickel-cadmium battery in 1901, that secondary batteries made an entrance. During the 20th Century, several different secondary battery chemistries were designed, the most successful one, the LIB, started in the 1960s and by several key persons [12], among them Stanley Whittingham, John B. Goodenough and Akira Yoshino who would win the Nobel prize in 2019.

The LIB has continued to dominate the R&D interest to this day. New chemistries are slowly starting to enter the scene, and first in line is the Na-ion battery, which chemistry is similar enough to the Li-ion battery, which means that the know-how and the production lines are more easily adapted, but different in one key aspect – it is a much more abundant element [13]. Other next-generation batteries have also attracted attention even if they are far from entering the market just yet, such as multivalent battery chemistries such as Mg, Al, and Ca metal [14].

In this chapter, the inner workings of a battery - both its cell components and the electrochemical reactions driving force - are explained, to give a fuller picture of all components that need to be considered when implementing new materials for new battery chemistries. Thereafter, an overview of the landscape of multivalent chemistries is presented, followed by a more in-depth description of Ca batteries. Finally, an explanation of metal anodes, as well as plating and stripping behaviour is described and put in to contrast with the more common anode material of today; graphite, and the intercalation mechanism.

2.1 Principles of rechargeable batteries

A battery provides electric energy by converting chemical energy through spontaneous chemical reactions [11]. This is realized through three main components: the electrodes; one negative (anode) and one positive (cathode), and the electrolyte. Together they make up an electrochemical cell (Figure 2.1), which is often referred to as a battery. The anode and the cathode contain the active materials of the battery and should always be kept physically apart to avoid short-circuiting. This is done by the separator absorbed with electrolyte, which typically is a liquid and traditionally consist of solvent and solute. The electrolyte's function is to shuffle ions between the electrodes, and by doing so enables the chemical reactions to occur at their surfaces. Lastly, the external circuit connects the two electrodes [15].

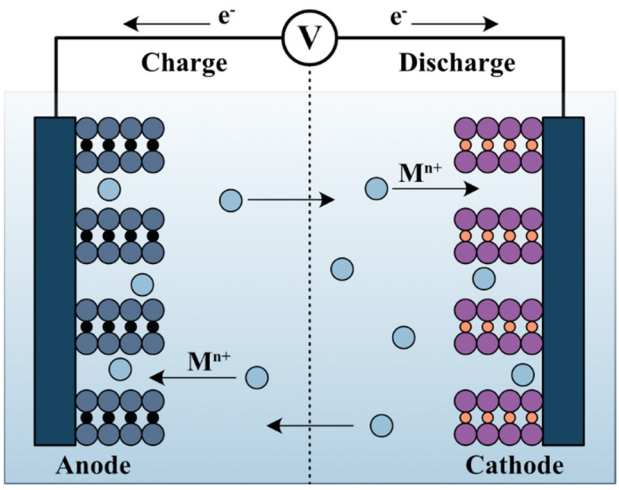

Figure 2.1. Electrochemical cell showing the electrolyte the anode, and the cathode connected to an external circuit (V), during charge (left) and discharge (right).

Rechargeable batteries will, depending on the state of charge or discharge, change which electrode is negative or positive. To minimize confusion, the electrode that is negative during discharge is always the one referred to as the anode and vice versa for the cathode [11]. During discharge, the anode gives up electrons, which go through the external circuit and to the cathode. At the same time, cations travel from the anode to the cathode through the electrolyte. The full reaction takes place during discharge,

$$M + X \rightarrow M^+ + X^- \tag{2.1}$$

where M typically is a metal and X an oxidant. This reaction can be divided into two half-reactions: the oxidation reaction at the anode,

$$M \rightarrow M^+ + e^- \tag{2.2}$$

and the reduction reaction at the cathode,

$$X + e^- \rightarrow X^- \tag{2.3}$$

The full reaction is reversible by placing an overpotential to the external circuit[11]. The amount of energy a battery can provide relies on how many ions the electrodes can accommodate and is referred to as the capacity,

$$Q = I \cdot t \tag{2.4}$$

where I is the current and t is the discharge time. The theoretical capacity is expressed in Ampere-hours (Ah) but is more practically expressed by the specific (gravimetric) capacity, which unit is capacity per electrode mass (mAh g^{-1}). Furthermore, for any reaction to occur, it must be energetically favourable as described by the Gibbs free energy,

$$\Delta G = -nFE^{\circ}_{cell} \quad (2.5)$$

where F is the Faraday constant and n is the number of electrons taking part in the chemical reaction. E°_{cell}, is called the cell voltage or the standard reduction potential (V), and is the potential difference between the two electrodes,

$$E^{\circ}_{cell} = (E_{red} - E_{ox}). \quad (2.6)$$

The energy (E) of the cell is then a function of the cell voltage and the capacity,

$$E = \int_0^Q E^{\circ}_{cell}(q)dq. \quad (2.7)$$

The energy is expressed in Watt-hours (Wh) but is more often reported as the specific energy density (Wh/kg) or the volumetric energy density (Wh/L). Of equal importance is the speed of the charge and discharge, which is expressed by the power,

$$P = E^{\circ}_{cell} \cdot I \quad (2.8)$$

where I is the current passed through the cell. The power as the unit Watts (W), and is more often reported in the form of the power density, either as W/kg or W/L.

In the search for battery chemistries with higher cell operation voltages, and therefore increasing the energy and power density, the standard reduction potential of the cathode has been pushed higher [2], effectively expanding the potential window. However, the development of electrolytes has at large been neglected, which has pushed them to operate outside their electrochemical stability limit [16]. The electrolytes will then start to chemically break down, though, in many modern electrolytes it is designed to do so [17], as the decomposition products will attach to the electrode surfaces, creating a new beneficial layer called the solid electrolyte interphase (SEI) [18].

Typically, the name SEI is only used for the interphase at the anode, while any distinct functional interphase created at the cathode is called the cathode electrolyte interphase (CEI) [19]. The SEI is conductive to ions but insulation to electrons [20] and creates a barrier between the surface of the electrode and the electrolyte, which effectively hinders further breakdown of the electrolyte. As such it has become a crucial component in the development of longer cycle life and safer batteries [21].

2.2 Multivalent batteries

Multivalent batteries have been part of the overall history of batteries from the very beginning, for example, the first commercial primary battery Zn/MnO_2 [14]. The novel multivalent batteries of research interest today are mostly Al, Ca, and Mg batteries, which have their own set of advantages and challenges. Compared to Li, Ca has a volumetric capacity not much different. However, Mg and Al there are approximately 2 and 4 times more performant, respectively [5], [14]. Ca has compared to Mg and Al, relatively low standard potential vs. the

standard hydrogen electrode (SHE) (Table 2.1), which gives Ca the potential for high operation voltages for CaBs [5]. One of the major challenges on the other hand is the diffusion of divalent ions is very sluggish, owing to the strong coulombic interactions of the cations due to their high polarising power [22].

In multivalent metal anodes, the layers formed are both insulating toward electrons and ions, hence disabling any form of charge transfer. This means that there are only two ways to make reversible multivalent batteries, either the layers must be controlled, for example by clever electrolyte design which creates SEIs that are not ionically isolating, or the electrolytes must operate inside the stability window, and therefore not break down and create layers in the first place [7].

However, the lower self-diffusion barriers at the anode interface do seem to lead to the safer use of Mg and Ca metal electrodes [22], which have shown to be much less prone to dendritic growth, compared to Li metal [6], [22]. While Mg, Al, and Ca have several challenges and motivations in common, they have largely different levels of maturity. Mg has been around and researched for 20+ years and Al has been picking up in recent years, and Ca is still in the very early days [14].

Table 2.1. Standard potential for selected metallic elements.

Metallic element	Electrode reaction	Standard potential/V vs. SHE
Li	$Li^+ + e^- \rightarrow Li^0$	-3.05
Cs	$Cs^+ + e^- \rightarrow Cs^0$	-3.03
Rb	$Rb^+ + e^- \rightarrow Rb^0$	-2.98
K	$K^+ + e^- \rightarrow K^0$	-2.93
Ca	$Ca^{2+} + 2e^- \rightarrow Ca^0$	-2.87
Na	$Na^+ + e^- \rightarrow Na^0$	-2.71
Mg	$Mg^{2+} + 2e^- \rightarrow Mg^0$	-2.37
Al	$Al^{3+} + 3e^- \rightarrow Al^0$	-1.66
H_2	$2H^+ + 2e^- \rightarrow H_2$	0.00

2.2.1 Magnesium batteries

The first prototype of Mg metal batteries was reported in 2000 [23] and has since then gained research interest. The main bottleneck is trying to find good electrolyte designs at the same time as the development of new cathode materials [5]. The most successful electrolytes early on were either Lewis acids or Grignard regents, or a combination of the two [24]. Rather recently, the $Mg[B(HFIP)_4]_2$ salt was synthesized, which when added in DME showed high conductivity and great coulombic efficiency in magnesium batteries [25]. On the cathode side, the insertion cathode types developed for Li-ions are not suitable for the divalent Mg cation. Some successes have been found with conversion cathode materials, such as sulphur, but they ultimately suffer from low operation voltages. Mg batteries are still at the laboratory level and more still needs

to be done to find good combinations of electrolytes and cathode materials, to build realistic full battery cells [24].

2.2.2 Aluminium batteries

Aluminium batteries are, despite being multivalent like Mg and Ca, very different from the other two. Uniquely the Al ion is typically part of the anion complex, such as $[AlCl_4]^-$, rather than as a cation. This creates challenges regarding intercalation into cathode materials [5]. The biggest motivation for Al batteries, apart from their large abundance, is the mature production line of the raw material, which neither Mg nor Ca has [14]. Still, a sombre perspective was recently published [26], on the current state of the current aluminium research, highlighting the difficulties of corrosion, and urging researchers to completely rethink electrolyte concepts and cathode materials.

2.2.3 Calcium batteries

Calcium already existed in battery chemistries as an additive in Pb/acid batteries in 1935, but as a metal anode it was never successful, and after reporting from Aurbach et al. in the 1990s reported that Ca plating and stripping were essentially impossible [8], all research on the element essentially died out. However, this was proven wrong in 2016 by Ponrouch et al.[9] who managed to achieve stable plating and stripping using $Ca(BF_4)_2$ in EC:PC at elevated temperature. Since this pivotal breakthrough Ca-batteries have attracted more interest.

Just as Mg, electrolytes, and cathodes need to be developed simultaneously, and unfortunately just as both Mg and Ca can make use of the know-how from LIB research, taking concepts from Mg and using it for Ca is not completely transferable either. Mg electrolytes that have found success in Grignard regents have no calcium analogues available [7]. In fact, the lack of commercial Ca-salts [14], is a limiting factor overall, which combined with the desire to make rechargeability possible at room temperature, was the main quest in the immediate year following the proof-of-concept. First to report on room-temperature deposition was Wang et al., in 2018, where they used $Ca(BF_4)_2$ in THF[27]. Following along, also at room temperature, two groups simultaneously synthesised and reported on the successful plating and stripping of Ca using $Ca[B(HFIP)_4]_2$ salt in DME [28], [29].

2.3 Anodes

While there are different types of anodes; intercalation, metal, alloy-based and conversion-reaction-based anodes [30], the focus herein will be on the first two. Intercalation anodes are by far the most popular in LIBs, and work by storing the ions inside the host material (Figure 2.2). Metal anodes, on the other hand, have significantly larger specific capacity, and work by storing energy by planting the metal ion directly to the surface. Furthermore, intercalation into host materials happens at a higher potential than plating on to metal anodes, which means that intercalation-types cannot store as much energy. Consequently, moving from intercalation-based anodes to metal anodes would lead to much higher theoretical energy density.

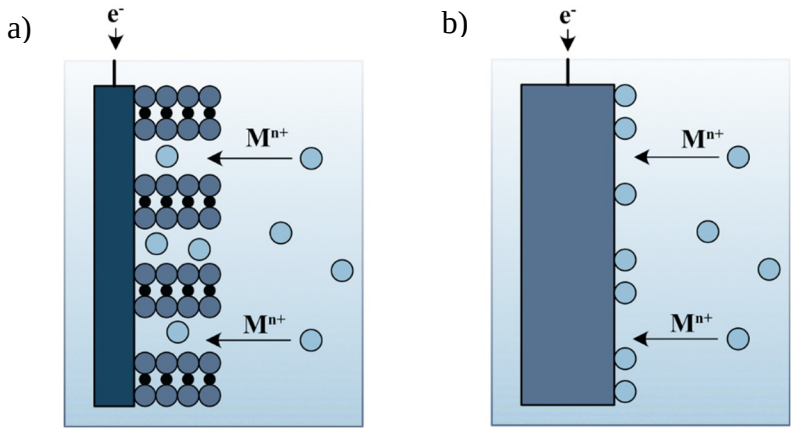

Figure 2.2. Energy storage through a) intercalation of ions and b) plating metal ions directly to the metal anodes.

2.3.1 Intercalation anodes

Intercalation anodes are made of host materials with an open structure, which provides a place for ions to be intercalated, without chemically reacting with said ions. The most successful one for Li^+ is graphite (372 mAh g^{-1}), which has a structure which consists of endless sheets of fused hexagonal rings (known as graphene) [31]. The benefit of using Li^+ is that it is a small ion (Table 2.2) and therefore easily fits into the open structure. However, bigger ions like K^+ have also been successfully intercalated, though not without distorting the structure which can cause changes in diffusion properties, redox behaviour, and interfacial compatibility [32]. Na^+ which ionic radii lay between these two, struggles to desolvate from the electrolyte solution because of its high Lewis acidity, making intercalation more troublesome [30].

Looking at multivalent ion charge carriers, the great benefit of them is that only half or one-third amount of the ions need to be transferred to the host material to reach the same capacity compared to monovalent ion charge carriers [33]. However, the mobility of multivalent ions is sluggish due to their charge. Furthermore, the diffusion of Ca^{2+} is affected by the relatively large ion radius [34]. Still, much of the hope for multivalent intercalation anodes hangs on the hope of finding host materials that can accommodate the multivalent cations, while still not reaching the much larger specific capacities of metal anodes.

Table 2.2. Ionic radii for selected cations [35].

	Cation							
Parameter	Li^+	Na^+	K^+	Rb^+	Cs^+	Mg^{2+}	Ca^{2+}	Al^{3+}
Ionic radius (Å)	0.76	1.02	1.38	1.52	1.67	0.72	1.00	0.54

2.3.2 Metal anodes

The great advantage of lithium metal and what has given this metal its high energy density, is its low electrode potential (Table 2.1). However, the great drawback is its extreme reactivity to

other species, which in the battery will lead to dendritic formation on the anode surface. Dendrites are needle-like structures which start to form when the electric field applied across the surface is not completely smooth. As no surface can possibly be totally homogenous, irregularities will always happen and cannot be avoided. The roughest parts will have the highest voltage and will be at the places at which cations will prefer to deposit as it is more energetically favourable. The dendrites have the potential to grow to such a length that the electrodes will connect internally, which leads to short-circuiting. In the worst case, this can lead to fires or explosions. Furthermore, dendrites can be broken off during the stripping process, where the isolated particles created are referred to as "dead Li^0". Dead Li^0 is even more reactive than dendrites attached to the electrode surface, and as such also more prone to dangerous outcomes [31].

A large part of the attraction of using multivalent elements comes from the possibility of using metal anodes. While Ca (1 337 mAh g^{-1}), Mg (2 206 mAh g^{-1}), and Al (2 980 mAh g^{-1}) have lower specific capacity than Li metal (3 856 mAh g^{-1})[31], they are much less prone to dendritic growth. In fact, while Li metal has shown dendritic growth at current densities as low as 1 mA cm^{-2}, Ca and Mg metal there is no dendrite formation below 20 mA cm^{-2} [6]. While not as much effort to hinder dendrite formation is needed for multivalent metal anodes [30], more effort is needed to develop new electrolyte chemistries to hinder the formation of passivation layers [36].

Chapter 3

Electrolytes & interfaces/interphases

The relationship between electrolytes and interphases/interfaces is one of the most important and most complex parts of understanding the battery material chemistry, and this chapter aims to sort through some key concepts, with a special emphasis on MSEs.

3.1 Electrolytes

As the electrolyte is the transporter of ions between the electrodes, it needs to be ionically conductive. The easier the transportation is the more ionically conductive the electrolyte is. This largely correlates to the viscosity of the electrolyte, where the less viscous the electrolyte is, the easier it typically is for the ions to move [20]. This usually also means that the electrolyte should be liquid at the temperature range at which the battery is to be used [37]. This no longer holds completely true. In recent years, interest has been taken to solid-state electrolytes, which as the name suggests are solid and not liquid in the operation range of the battery [38]. Other electrolytes such as polymer and gel electrolytes, as well as MSEs and ionic liquids (ILs), also tend to have higher viscosities.

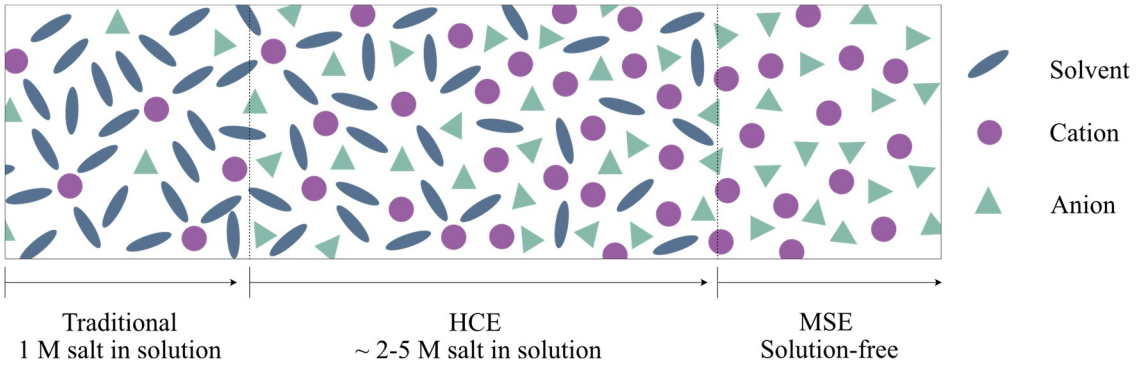

Figure 3.1. Local electrolyte structure as a function of salt concentration.

The concentration of the solute is also important to consider, as the concentration increases the ionic conductivity increases too, until a maximum is reached and then the conductivity starts to decrease due to the increase of viscosity. A traditional electrolyte has about 1 M salt in the solvent, however, in later years highly concentrated electrolytes (HCEs) (>2 M) have gained research interest (Figure 3.1). At this level of concentration, the cation and anions will start to form ion-contact pairs. In some cases, they are even super-concentrated (>5 M), at which point the solvent molecules will form clusters with the cations and anions, forcing the remaining ions in contact with each other [39]. This will create many unpredictable properties, much of which are not concentration-dependent, but rather dependent on the size of the ions, their charge (monovalent or multivalent), fluorination etc. These types of highly concentrated and super-

concentrated electrolytes have slowly started to bridge the definitions of liquid electrolytes and MSEs [20].

The stability of the electrolyte also needs to be taken into account. The stability here relates both to the electrolyte's thermal properties, but also the stability towards the electrodes. Assuming that the electrolyte should be a liquid – then it should not freeze in low-temperature battery application, and the opposite, in a hotter battery environment, it should not boil [17]. The wetting of the electrolyte on the electrode surface is also something to be considered. Poor wettability will lead to higher resistance for the charge transfer and lead to poor performance of the battery [17]. Finally, the electrolyte should preferably be non-toxic and economical [37].

3.1.1 Liquid electrolytes

Liquid electrolytes dominate the vast majority of the batteries on the market today. They consist of a solvent and solute (salt) and sometimes make use of additives. Solvents commonly used are propylene carbonate (PC), ethylene carbonate (EC), and dimethyl carbonate (DMC) to name a few, which have either high dielectric permittivity or low viscosity. There is no perfect solvent which will have all desirable properties, combining solvents is therefore very common [40], but even then, it is a matter of compromise. What all the solvent molecules in liquid electrolytes have in common, is that they assist the dissociation of the salt so that the cation and anion are free and can be transported independently [20].

The relationship between the ionic conductivity and the viscosity depends on how ions move in the electrolyte, which in turn depends on how mobile the ions are. The ion mobility can be described as the drift velocity, and it depends on two types of motion – diffusion and migration. Diffusion describes how ions move on their own, driven by a local uneven distribution of ions, which varies by time. On the other hand, when an external circuit is turned on, there will be a potential difference between the electrodes – the ions will then have a preferred direction and move according to the applied charge. This is migration, also sometimes called conduction. The diffusion in a system happens regardless of charge state, and can be related to the mobility, by the Einstein relation [41],

$$D = \mu k_B T \tag{3.1}$$

where D is the diffusion coefficient, μ is the mobility, k_B is the Boltzmann constant and T is the absolute temperature. This relation shows that the diffusivity is in direct correlation to the mobility of the ions. Combining Einstein's relation with Stokes's law, which describes the drag force which acts upon a spherical object, gives the Stokes-Einstein relation [41],

$$D = \frac{k_B T}{6\pi\eta r} \tag{3.2}$$

where η is the dynamic viscosity and r is the radius of the particle. This relation describes the diffusion of ions in a solvent. Furthermore, the diffusivity can also be understood through the conductivity, by the Nernst-Einstein relation [41],

$$\Lambda = \frac{z_i e_0 F}{k_B T}(D_+ + D_-) = \frac{z_i F^2}{RT}(D_+ + D_-) \tag{3.3}$$

where Λ is the molar conductivity, z_i is the valences of the ions, F is the Faraday constant and R is the gas constant. In this relation the independent contributions of the diffusivity from the anion and the cation are related to the conductivity, and as such the relation only holds true for very diluted electrolytes, where no ion-contact pairs are present. While ion-contact pairs can contribute to diffusion, they are electroneutral and thus, do not carry charge and cannot contribute to the migration of ions in the electrolyte [41]. A traditional electrolyte for batteries has about 1 mol/dm^3 of salt in the solvent, which is typically a concentration low enough to fully dissociate the ions, but still high enough for them to feel each other's Columbic effect [42].

3.1.2 Molten salt electrolytes

Molten salts are liquids that consist of only ions and where no molecular species are present. Ionic liquids, which are in all senses of the stated definition the same as molten salts, have a shared history, but developed later in parallel, by research groups not aware of each other's work [43]. This is where definitions become more complicated. Molten salts were from the very beginning developed for nuclear reactors to store heat [44]. Inherently this meant that the first molten salts were liquid at very high temperatures. Researchers in different fields of interest started to realise the benefits of having low melting salts [43], such as low volatility, large thermal, chemical, and electrochemical stability, and high electric conductivity [45]. At this point, in the late 80s to early 90s, molten salts and ionic liquids were not only referred to as such but names like 'ionic fluid' and 'liquid organic salt' were used as well [45].

Looking at the present day of how researchers choose to refer to their liquids composed of only ions, the general trend is still to categorise by temperature. It is common to draw a strict line between salts melting below 100 °C to describe ionic liquids and above as molten salts [45], however, others do not agree [43]. Furthermore, molten salts typically consist of inorganic cations such as Li^+, Na^+, K^+, Mg^{2+}, etc. Ionic liquids, instead, make use of large organic cations, to bring the salts melting temperature down to room temperature or lower [46]. Technically any single salt whose cations and anion can be dissociated by temperature can become a molten salt [20] (Figure 3.2). However, a special emphasis on eutectic compositions is regularly made for molten salts, which is a result of them often exciting in binary or higher-order systems [46]. Meanwhile, ionic liquids are typically used as they are or as a solvent combined with a dissolved salt [43].

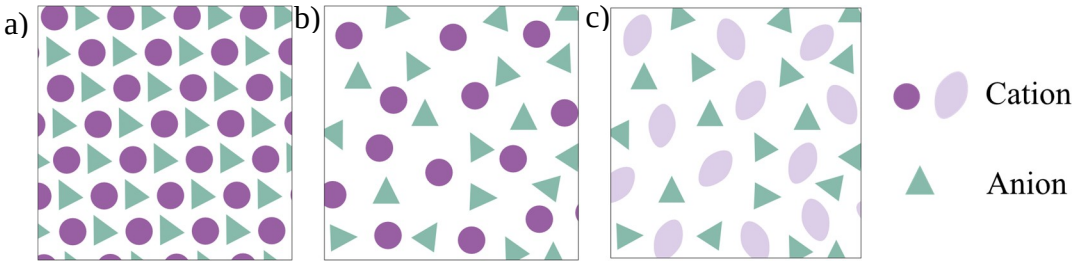

Figure 3.2. Visualization of a) a single salt, b) a molten salt, and c) an ionic liquid.

Here, the term MSEs is used intentionally, to first highlight the application (electrolytes) and the role they have in this work. Second, all cations used in various molten systems are either alkali metal ions like Li^+, Na^+ or K^+ or alkaline earth metals like Ca^{2+}, and therefore, inorganic. Hence, the chosen definition of molten salts versus ionic liquids, herein, is by types of cations rather than drawing a strict line by temperature.

Despite MSEs having no solvent molecules, and thus no liquid for the ions to diffuse through, the Stokes-Einstein equation ((3.2) still roughly holds true. This is related to the "voids" created in the MSEs because of the volume expansion (~10-20%) upon melting. This creates an uneven distribution in the long range which allows the ions to move. As the voids and the ions are roughly the same size, no other consideration is needed for the Stokes-Einstein equation. However, in the short-range MSEs are still ordered, which means that for the Nernst-Einstein equation ((3.3) a correction term for the ion-contact pairs must be added [41],

$$\Lambda = \frac{zF^2}{RT}(D_+ + D_-) - \frac{zF^2}{RT} D_{ion\ pair} \tag{3.4}$$

Systems of MSEs have been tested in different chemistries, from traditional Li-ion batteries [47] to next-generation battery concepts such as lithium-air [48], Na-ion [47] and Na-metal [49], [50], and Al-ion [51] and Al-metal [10]. Frequently, these molten salt electrolytes consist of different chloride salts, some with high melting points of around 350-500 °C [49], [50], others have successfully made use of $AlCl_3$, which forms large Al_xCl_{3x+1}– moieties, which brings down the melting temperature to 120 °C [51] or even 93 °C [10]. Combinations of binary and ternary mixtures of either bis(trifluoromethylsulfonyl)imide (TFSI) [52]–[54], bis(fluorosulfonyl)imide (FSI) [55]–[58] or (fluorosulfonyl)-(trifluoromethanesulfonyl)imide (FTFSI) [59]–[63] have also been explored in a series of articles and summarized [47], there it is shown that it is possible to bring down the melting temperature to as low as 36 °C, still only using inorganic cations.

3.2 Gibbs free energy

Consider a closed system, the first law of thermodynamics applies the mechanical principle of energy conservation to thermodynamic systems, by establishing that if a system undergoes any transformation, then, the variation of its internal energy U, is a summation of the heat exchanged with its surroundings, δQ, and the work spent or done on the system, δW, as follows,

$$dU = \delta Q + \delta W = \delta Q - P\,dV \tag{3.5}$$

Conversely, the second law of thermodynamics introduces entropy, another state function that determines whether a transition from one state to another occurs spontaneously. Therefore, while the first law introduces internal energy to discern allowable changes, the second law employs entropy to distinguish spontaneous transitions among these allowable changes. Thus, for an infinitesimal transformation involving a heat exchange with a reservoir at temperature *T*, the second law dictates that the change in entropy of the system obeys the following relationship,

$$dS \geq \frac{\delta Q}{T} \tag{3.6}$$

specifically, the entropy of a thermally insulated system can only increase or be stationary: $dS_{ins} \geq 0$ which means that the entropy increases during a spontaneous change. Consider now a system in thermal equilibrium at temperature, *T*. When a system undergoes a change and there is an exchange of energy with the surroundings,

$$dS - \frac{dq}{T} \geq 0 \tag{3.7}$$

If the energy is transferred as heat as constant pressure, P, and there is only expansion work, then $(dq = dH)_P$, and

$$T\,dS \geq dH \tag{3.8}$$

At constant enthalpy or constant entropy, the previous inequality can be written as,

$$(dS)_{H,P} \geq 0 \tag{3.9}$$

or as,

$$(dH)_{S,P} \geq 0 \tag{3.10}$$

respectively. On that account, at constant pressure, if the enthalpy of a system remains unchanged, the system's entropy must increase, as there can be no alteration in the entropy of the surroundings. Likewise, if the system's entropy remains constant, the enthalpy of the system must decrease, as this ensures an increase in the entropy of the surroundings. By introducing a state function, the Gibbs free energy can be written as,

$$G = H - TS \tag{3.11}$$

When the state of the system changes at a constant temperature, then,

$$\Delta G = \Delta H - T\Delta S \tag{3.12}$$

By its definition, Gibbs free energy is influenced by the interplay between the enthalpy change and the entropy change. For a pure system, like a single salt, which goes through a phase change, the corresponding equation is,

$$\Delta G_{fus} = \Delta H_{fus} - T\Delta S_{fus} \tag{3.13}$$

For compositions, either binary or of higher order, such as MSEs, there is a contribution of both fusion and mixing. Here, only the mixing effect is assumed,

$$\Delta G_{mix} = \Delta H_{mix} - T\Delta S_{mix} \tag{3.14}$$

where the entropy of mixing is given by

$$\Delta S_{mix} = -nR \sum_i x_i \ln x_i \tag{3.15}$$

where n is the total number of moles, R is the gas constant and x_i is the molar fraction of the species i. Because $ln\ x < 0$, it follows that $\Delta S_{mix} > 0$ for all compositions. Consequently, the addition of multiple components to increase ΔS serves as a tactic to counterbalance ΔH, hence decreasing the free energy. The high-entropy effect involves the addition of extra components in the system [64].

3.2.1 High entropy electrolytes

The interest in intentionally increasing a system's entropy stems from high entropy alloys (HEA) [65], which defines high entropy as a system composed of five or more components, of which at least make up 5% of the whole [66]. When alloys are in this compositional region, interesting properties start to emerge, such as high hardness and superb specific strength, superior mechanical performance at elevated temperatures, and exceptional ductility and fracture toughness at cryogenic temperatures [67]. In the last years, the interest in high entropy has expanded to other types of materials, such as ceramics [68] and for specific applications, such as energy storage [69].

In terms of electrolytes, high entropy has started to be explored as well, even if a strict definition of high entropy electrolytes (HEEs) is still quite ambiguous. Some refer to their system as having higher entropy by using several solutions [70], [71], others do so by using more than one salt [72], and others do both [73]. Whether it is truly high entropy or not in the strict sense as seen in HEAs is not of as much interest, as to conclude that enough articles have been published on the subject to accept that electrolytes go under different definitions. Interesting properties due to the high entropy effect have been found for HEEs. By using more than one solvent the cation mobility was increased [70] and hence led to higher diffusivity and conductivity. This was proven to be due to smaller clustering of cations [74]. Furthermore, increased entropy of a system lowered the freezing temperature of the electrolyte and increased the operation temperature of the battery cells [70].

In the MSEs community, the high entropy effect is not talked about directly, even though in binary and higher order systems, the lowering of melting temperature is a direct effect of the increased entropy of mixing. As MSEs originate from MSs, it is in the nature of the community to combine different components, however, most do not extend past ternary systems. The complexity of combining different cations, anions and their corresponding charges, instead raises the question of the effect of the internal energy of the system.

3.2.2 Charge symmetry & asymmetry

It is of great importance to understand which combinations of salts will create homogenous mixtures for MSs. This is largely attributed to the enthalpy of mixing, and as such MSs can be created in different configurations and levels of complexity (Figure 3.3). Two things need to be considered: (1) If the salts mixed contain a common cation combined with multiple anions (multi-anionic) or contain a common anion combined with multiple cations (multi-cationic) and (2) if all ions in the mixtures have the same charge (symmetric) or different charges (asymmetric). Keeping this in mind, mixtures can be classified into three different categories with increasing complexity [75]:

I. Mixtures with symmetric charge structures that are either multi-anionic or multi-cationic.

II. Mixtures with asymmetric charge structures that are either multi-anionic or multi-cationic.

III. Mixtures with either symmetric or asymmetric charge structure with no common cation or anion.

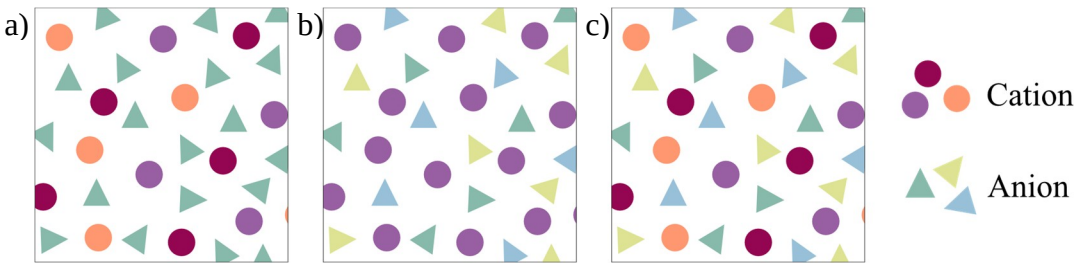

Figure 3.3. MSE of a) multi-cationic, b) multi-anionic and c) mixed cations and anions systems.

The change in enthalpy is related to the ionic radius [76]. Multi-cationic mixtures in category I do in general have a more ideal enthalpy of mixing if the species are not too different in size. Furthermore, when comparing multi-cationic mixtures of analogous anions, the variation in the enthalpy of mixing is small. For analogous multi-anionic systems, the same is true, as long as the relative cation size difference is small. Looking more closely at multi-anionic systems, the larger the difference between the anions in the system, the more endothermic the enthalpy of mixing [75].

In category II, the mixing of multivalent and monovalent cations has been shown to create a “competition" between them for the common anion. This is driven by the polarizing power of

the cations. Small cations like Li^+ and to some extent Na^+, mixed with multivalent cations have small enthalpies of mixing and the formation of complex anions is less likely. While large cations like K^+, Rb^+ and Cs^+ mixed with multivalent cations have more negative enthalpy of mixing and are more prone to the formation of complex anions. For multivalent cations, the larger polarizing power of Mg^{2+} relative to that of Ca^{2+}, makes Mg^{2+} more prone to complex anions [75].

When making mixtures with no common cation or anion (category III), the ideal mixing of salts is,

$$AX + BY = AY + BX \tag{3.16}$$

where salt *AX*, containing cation *A* and anion *B*, is mixed with salt *BY*, containing cation *B* and anion *Y*, would create the same mixtures as combining salt *AY* and *BX* (Figure 3.4) [75]. However, often mixtures are not ideal, hence, the species created will depend on which ones are energetically favourable. Typically, small cations are drawn to small anions, and large cations are drawn to large anions [77], which will create short-range ordered clusters in the melt. Therefore, when mixing cations and anions simultaneously, the choice of which ones needs to be carefully considered.

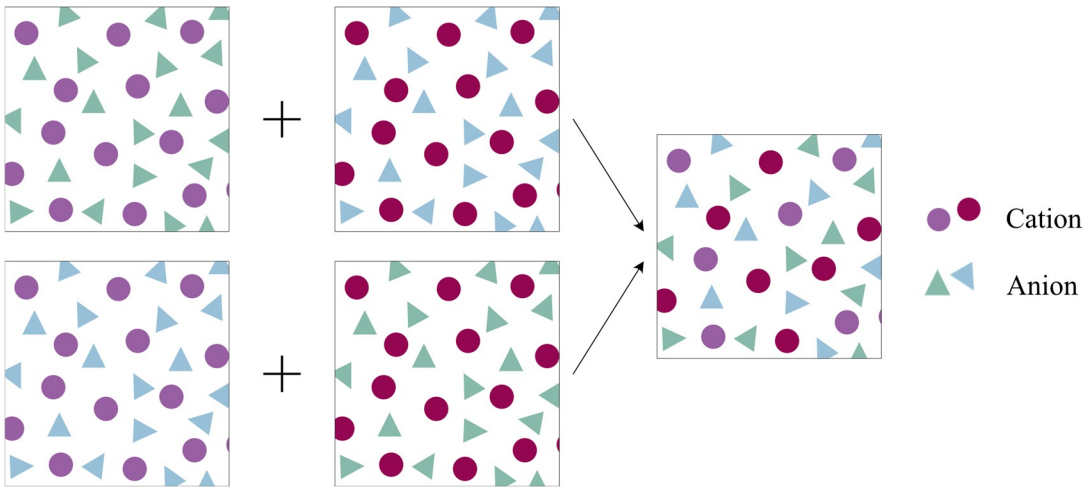

Figure 3.4. Ideal mixing of salts in category III.

3.3 Interfaces/Interphases

An interface is the intersection between two physically distinct phases. It does have its own set of unique properties, due to the electric charge buildup between the two phases, called the electric double layer. As such it does not behave as the bulk electrode or the bulk electrolyte [78]. When the electrolyte decomposes, the species attach to the surface of the electrodes and start to form an interphase, it becomes its own distinct phase. This means that the system now has one more interface – one between the electrode and the interphase, and one between the interphase and the electrolyte (Figure 3.5). This statement holds true for graphite and mental anodes, but becomes more ambiguous for transition metal oxides, as they often

experience a conversion type of layer, which is not completely distinct from the electrode material [79].

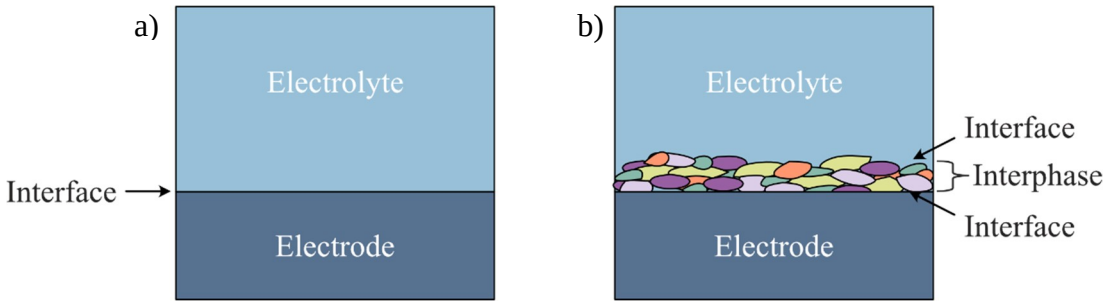

Figure 3.5. Electrode and electrolyte acting a) inside the ESW and b) outside the ESW.

The interphase that is beneficial to the battery cell, the SEI, must be stable enough to not dissolve back into the electrolyte, as well as being inactive to electrons. While metal deposition is also formed at the electrode surface, it is not a new distinct phase and is also conductive to electrons, which means it is not an SEI [78]. As the SEI is composed of very diverse products, it is often uneven - something which is not desirable as it increases the likeliness of dendrite formation. The layer is typically somewhere between 2-50 nm, as anything less than 2 nm will not stop the tunnelling of electrons, and anything thicker than 50 nm will make ion conduction limited [79].

The beneficial interphases, the SEI and CEI, have one crucial assignment and that is to extend the electrochemical stability window of the electrolyte (Figure 3.6). The limit of the electrolyte can be defined as the difference between the lowest unoccupied molecular orbital (LUMO) and the highest occupied molecular orbital (HOMO). Electrons at a higher energy level than the LUMO will be transferred to the electrolyte which will cause a reduction decomposition to occur. Accordingly, if electrons are at a lower energy level than the HUMO, electrons will instead be extracted from the electrolyte and oxidation decomposition occurs [79].

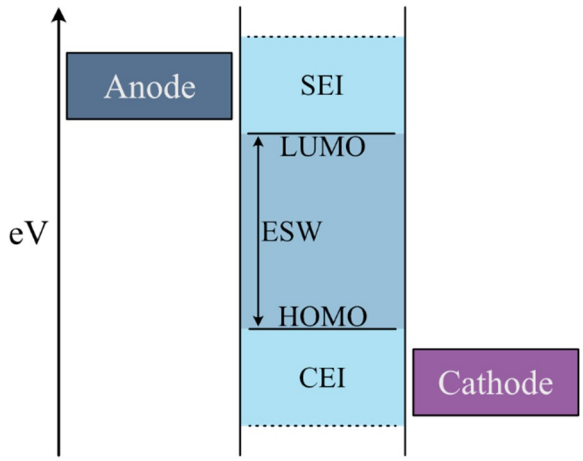

Figure 3.6. The electrolyte stability window.

The most vulnerable species in the system will decide the oxidation and reduction limit, however, the respective limits do not necessarily come from the same species [78]. It is also shown that the stability of the species depends on operation temperature, as higher temperature means higher likeliness of dissolving. Typically, the least soluble species are inorganic ones, placing organic ones as the more vulnerable. Furthermore, moving beyond Li creates other circumstances. Na is in general much more soluble, meaning that the electrolyte will not be protected by the SEI layer and will continue to decompose. K is about as soluble as Li [79]. Multivalent elements like Mg and Ca, do not have the same problem, as the phases formed by these products instead tend to be very stable [6]. This means that the phase created is insulating to both ions and electrons, which makes it a passivation layer that hinders further charging and discharging, and as such is no longer a functional SEI-layer [79].

Because of the different ways the SEI behaves depending on the components it is formed from, the ionic migration though the layer is for many systems the rate-determining step (RDS) [21]. In interphases, the ions are immobilized and for them to migrate from one coordination to the next, they first need to free themselves and hop. Multivalent ions have a hard time doing so because of the very strong Columbic interactions with the surrounding species [79]. Therefore, it was long believed that multivalent battery chemistries should be interphase-free [31]. While making SEI-free batteries would get rid of the resistance of the RDS of the system and lead to excellent power density and reversibility, the trade-off would be mediocre energy density [79]. Still, much of Mg and Ca research began here, particularly for Mg with Grignard's reagents. However, the anodic resistance was weak and there were not many other solutions to choose from. Eventually, it was realized that multivalent batteries can work with a SEI present as well [31]. In Ca in particular, it has been found that fresh SEI-layers that are disordered and contain many defects, enable Ca^{2+} migration, however, during storage when the SEI-layer have become more ordered, thicker and with fewer defects, the layer is entirely passivating [21].

Chapter 4

Experimental

Here the experimental methods used are presented alongside any adaptation needed for molten salt electrolyte (MSE) studies.

4.1. Preparation of molten salt electrolytes

Three main types of MSEs have been studied, all focusing on the Ca^{2+} as the conducting species: A multi-anionic MSE consisting of three different Ca-salts, a multi-cationic MSEs consisting of five different TFSI-salts and finally a multi-cationic MSEs consisting of up to four different FSI-salts. While it would be desirable to have eutectic compositions of the MSEs, the complexity and the time-consuming task of experimentally finding the eutectic point for ternary and quaternary systems, has led to the choice of creating equimolar compositions. The MSEs are prepared inside an argon-filled glovebox by manually grinding the salts together with a mortar and pestle for ~15 minutes, to create even and smooth powders.

4.1.1 Multi-anionic Ca^{2+}-based MSE

The multi-anionic MSE, $Ca[FSI,TFSI,NFSI]_2$ (Table 4.1), consisting of $Ca(FSI)_2$ (Provisco CS, 99.0 %), $Ca(TFSI)_2$ (Solvionic) and $Ca(NFSI)_2$ (Provisco CS). Before the grinding process, Ca-salt were dried in a vacuum Büchi oven, at temperatures adjusted to their melting temperatures, as follows: $Ca(TFSI)_2$ was dried at 120 °C for 24 h and $Ca(NFSI)_2$ at 100 °C for 48 h. $Ca(FSI)_2$ was used as received.

4.1.2 Multi-cationic TFSI-based MSE

One quinary system containing $Ca(TFSI)_2$ (Solvionic), LiTFSI (Nippon ShokuBai Co.), NaTFSI (Solvionic, 99.7%), KTFSI (Nippon ShokuBai Co.) and CsTFSI (Solvionic, 99.7%), was created as well. All salts were dried in a vacuum Büchi oven at 80 °C for 72 hours.

4.1.3 Multi-cationic FSI-based MSEs

Four multi-cationic MSEs, three ternary and one quaternary (Table 4.1), were prepared by combining $Ca(FSI)_2$ (Provisco CS, 99.0 %) with the analogous LiFSI (Nippon ShokuBai Co.) NaFSI (Solvionic, 99.7%), and KFSI (Nippon ShokuBai Co.). All salts were dried in a vacuum Büchi oven, at 80 °C for 72 hours, apart from $Ca(FSI)_2$ which was used as received. The molten salt electrolytes were given the names [Ca,Li,Na,K]FSI, [Ca,Li,Na]FSI, [Ca,Li,K]FSI, and [Ca,Na,K]FSI as represented by the different cations and the anion contained in each of them. To confirm that these molten salt electrolytes have eutectic points containing Ca, four

corresponding mixtures without $Ca(FSI)_2$ were recreated [57], but in equimolar compositions, as well.

Table 4.1. All MSEs studied.

Category	MSEs	Single salts
Multi-anionic Ca^{2+}-based	$Ca[FSI,TFSI,NFSI]_2$	$Ca(FSI)_2$, $Ca(TFSI)_2$, $Ca(NFSI)_2$
Multi-cationic TFSI-based	[Ca,Li,Na,K,Cs]TFSI	$Ca(TFSI)_2$, LiTFSI, NaTFSI, KTFSI, CsTFSI
Multi-cationic FSI-based	[Ca,Li,Na,K]FSI	$Ca(FSI)_2$, LiFSI, NaFSI, KFSI
	[Ca,Li,Na]FSI	$Ca(FSI)_2$, LiFSI, NaFSI
	[Ca,Li,K]FSI	$Ca(FSI)_2$, LiFSI, KFSI
	[Ca,Na,K]FSI	$Ca(FSI)_2$, NaFSI, KFSI
Multi-cationic FSI-based (references without Ca^{2+})	[Li,Na,K]FSI	LiFSI, NaFSI, KFSI
	[Li,Na]FSI	LiFSI, NaFSI
	[Li,K]FSI	LiFSI, KFSI
	[Na,K]FSI	NaFSI, KFSI

4.2 Thermal gravimetric analysis

Thermal gravimetric analysis (TGA) is a technique where mass change is measured under a controlled temperature program, where the temperature is either continuously increased (dynamic) or kept at a constant temperature (isothermal) [80]. This way it is possible to find out at which temperature or at which time a material starts to decompose, and the result is a typical step in the curve, as shown in Figure 4.1. While this figure shows only one step, a material can have several steps.

When studying decomposition from TGA data, it is most common to look at where 1% and/or 5% of mass loss occurs. For very pure materials, the 1% mark gives a good indication of when the decomposition starts to occur. However, if any impurities are present, in the material or the crucible holding the sample, that decay before the main reaction, it can give deceptive results. Hence, the 5% mark is often a more secure way to see the material break down.

TGA was performed on all single salts and MSEs, using a TG 209 F1 Iris from Netzsch, in the range of 25 °C to 500 °C at a heating rate of 5 °C/min. To protect the hydrophilic samples, sealed aluminium pans with pinholes in the lids were used and filled with ca. 5-12 mg of sample inside an argon-filled glovebox. The MSEs are tested in their powder form, directly from the preparation step, but melt far before the decomposition, and still give an accurate decomposition temperature.

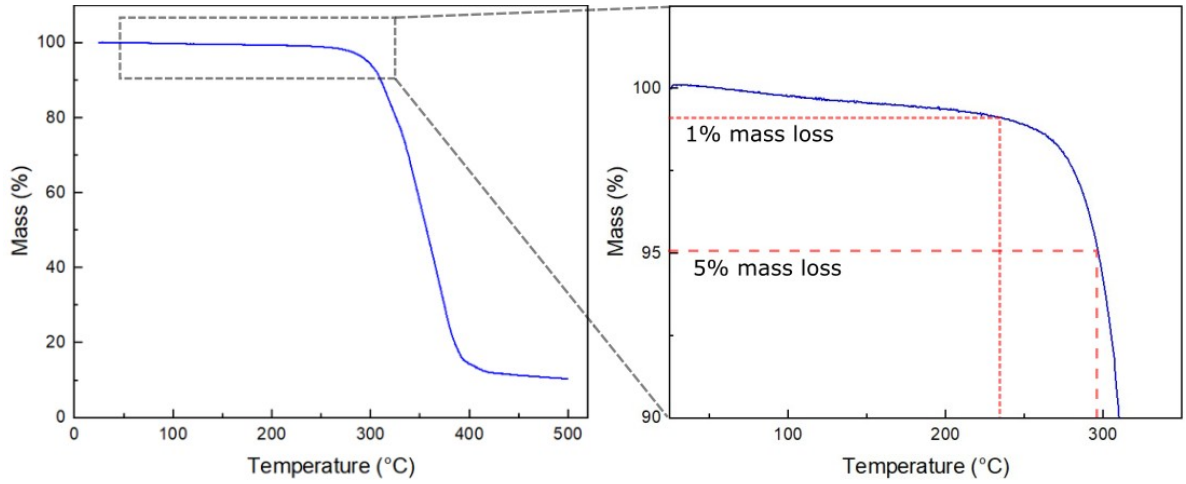

Figure 4.1. TGA trace showing a) overall behaviour and b) details of the 1% and 5% mass losses.

4.3 Differential scanning calorimetry

Differential scanning calorimetry (DSC) is a technique in which a sample, which can be any type of material, and an inert reference, typically an empty pan, are placed on their individual sample holder in the same furnace [81]. The goal is to keep the heat flux to both even, any deviations will give a signal which creates a peak in the thermal analysis curve. When the sample melts, an endothermic reaction occurs and the DSC responds by increasing the heat flux to the sample, so that the heating of the sample and the reference are even again. On the other hand, if the sample crystallises, the opposite happens; the reaction is exothermic, and the DSC needs to respond by decreasing the heat flux to the sample. The most common reactions that can be studied with DSC, which can be seen in Figure 4.2, are glass transitions, T_g, crystallization T_c and melting T_m.

During the glass transition, no formal phase change occurs, only the relaxation of a phase, which consequently will appear as a step in the thermal analysis curve. The T_g can be defined in different ways, such as the onset or the endpoint of the transition, the most common way, which is the way defined in this thesis is by the midpoint. As opposed to the T_g, the T_m, of the system is defined as the onset of the reaction. As also seen in this figure, the area between the melting peak and the baseline corresponds to the enthalpy of fusion, ΔH_{fus}, for a pure system. For MSEs the same area, herein, is designated as the enthalpy of mixing, ΔH_{mix}.

When the entropy ΔS in a system is increased, such as in higher-order molten salts, the corresponding curve tends to follow one or two ways. Either the salts mix well together and the corresponding melting peak will look more or less like the melting curve in Figure 4.2, or if the salts do not mix fully with each other, two or more separate peaks for each salt will be seen.

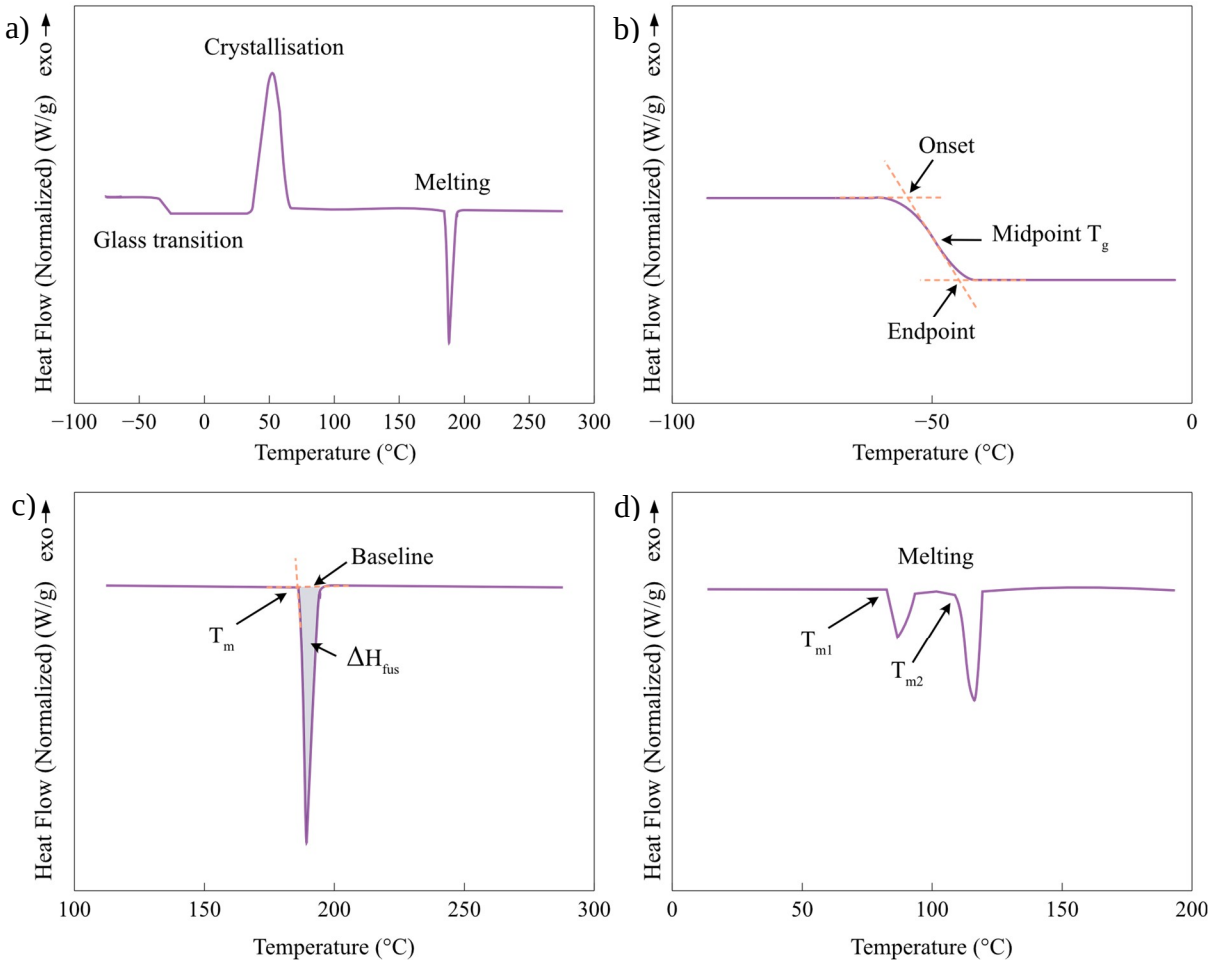

Figure 4.2. A typical DSC trace showing a) glass transition, crystallisation and melting for a single salt, b) a close-up of glass transition with onset, endpoint and midpoint, c) close-up of the melting point and the change in enthalpy, and d) melting peaks for a MSE with separate melting points.

DSC was performed using a DSC250 from TA Instruments. Sealed Tzero aluminium pans with ca. 5-12 mg of the sample were prepared in an argon-filled glovebox and compared with empty pans of the same sort, and then tested under flowing helium gas, 50 ml/min. For the T_m of single salts and MSEs, the initial heating curves taken between -50 °C to 200 °C (300 °C for $Ca(FSI)_2$) at a heating rate of 5 °C/min were used. For the T_g of molten salt electrolytes, new samples were prepared and heated at 10 °C/min to 150 °C and kept there for 30 minutes, before being cooled down at 10 °C/min to -100 °C, kept for 5 minutes, and then heated at 5 °C/min to 200 °C. Only the last heating curve is included to show the T_g.

4.4 Raman spectroscopy

With Raman spectroscopy, it is possible to identify the vibrational frequencies of a material. This means that characteristics such as compositions, interactions, and phase of a material, can be determined. While some materials are Raman inactive, such as metals, all materials that are Raman active, have their characteristic spectra. This means Raman can be used for molecular identification [82]. Furthermore, Raman can be used mapping tool to see gradients in a material,

as well as *operando* where it is possible to follow peaks that appear and disappear during charge and discharge during battery cycling.

When light impinges on a sample with the frequency ν_0, most of it is passed through the sample. A small amount, roughly 1/1000 of the resulting photons scatter, and do so in all directions, either elastically or inelastically, as can be seen in Figure 4.3. The photons that scatter elastically, that is, when the frequency in (v_0) and the frequency out (v_0), are the same, is called Rayleigh scattering. The photons that do not scatter with the frequency v_0 have instead scattered inelastically, which means that the material has absorbed some of the light and is therefore either greater than (Stokes) or less than (Anti-Stokes) the frequency v_0. The energy at which the photons scatter depends on the vibrational motion of the atoms. Depending on the motion, the consequent vibration is categorized in different modes, for example, bending (change of angle between two atomic bonds) or stretching (vibration in the same direction of atomic bonds), among others. While both Stokes and Anti-Stokes scattering are part of Raman scattering, they give the same information, but the intensity of the Stokes scattering is stronger and therefore more commonly used [82].

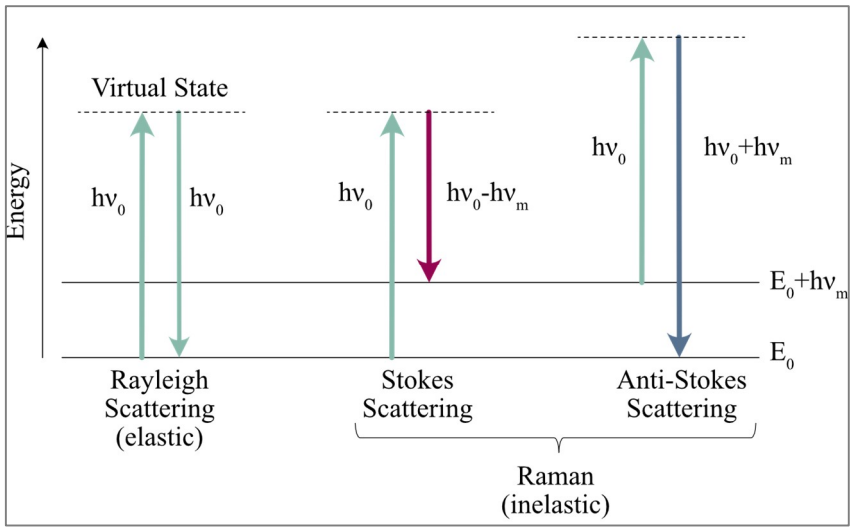

Figure 4.3. Schematic energy diagram showing the principles of elastic (Rayleigh) scattering and inelastic (Raman) scattering.

In this thesis, the FSI anion is present in several molten salt electrolytes, there a typical spectra of LiFSI can be seen in Figure 4.4. All single salts and molten salt electrolytes have been studied using a FT-Raman from Bruker. The molten salt electrolytes were placed in glass vials in powder form, and melted in a heated cell, at a temperature above their melting point (T_m + 50 °C), there they were kept for ~1 hour, after which spectra were taken. Thereafter, the samples were cooled down to room temperature and new spectra were taken. Furthermore, the samples were stored in an argon-filled glovebox for ~1 week and new spectra were taken at room temperature.

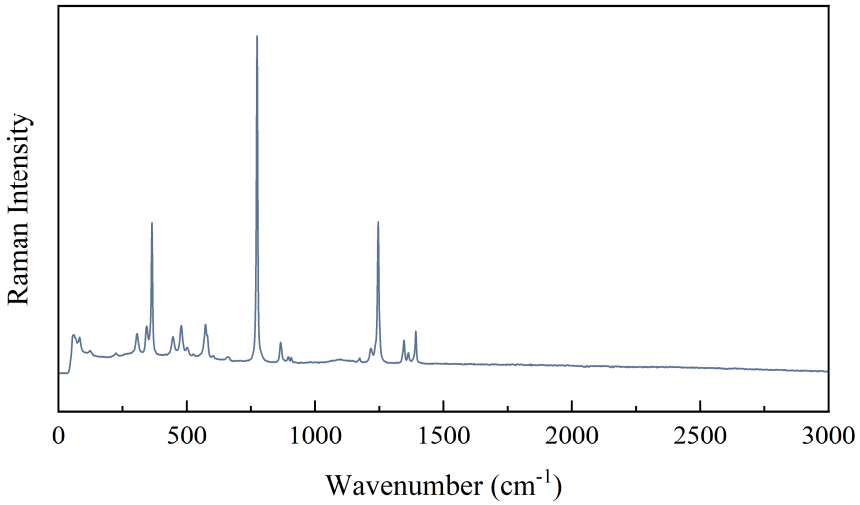

Figure 4.4. An example of a Raman spectra, here showing LiFSI.

Chapter 5

Results and discussion

In this chapter molten salt electrolytes for calcium batteries are presented in the first three subsections, followed by predictions of solubility of SEI-spices in the last subsection.

5.1 Multi-anionic Ca^{2+}-based MSE

For future battery tests containing Ca metal anodes, the charge carrier of interest is Ca^{2+}, it was thus of interest to create a MSE containing only Ca-salts. The chose of salt feel on the relatively low melting salts of FSI, TFSI and NFSI anions. This MSE is multi-anionic and has a symmetric charge structure, which does not make it a simple system but still makes it one of the least complex MSEs presented. In Figure 5.1, TGA and DSC traces of the single salts and the MSE $Ca[FSI,TFSI,NFSI]_2$ are seen. The T_d of the single salts are all well over 300 °C, while for the $Ca[FSI,TFSI,NFSI]_2$, 5% of the mass loss is reached already at 246 °C. Ca^{2+} exhibit strong Coulombic attraction, practically due to its relatively small size, but mostly due to its divalent nature. Therefore, it is quite surprising to see that a combination of Ca-salts produces a lower T_d than the single salts.

Of all the single salts, $Ca(NFSI)_2$ got the lowest T_m at 189 °C, followed by $Ca(FSI)_2$ at 240 °C and $Ca(TFSI)_2$ at 330 °C. Furthermore, $Ca(FSI)_2$ show a crystallization peak at 181 °C before it melts. $Ca[FSI,TFSI,NFSI]_2$ show a comparably small peak at temperatures which are hard to properly designate. While charge symmetrical multi-anionic MSEs in general, show small enthalpies of mixing [75], the absence of any clear melting behaviour, together with the lowered T_d of this system, indicates that this combination of salts does not form homogenous melts. Consequently, the $Ca[FSI,TFSI,NFSI]_2$ electrolyte was not studied further.

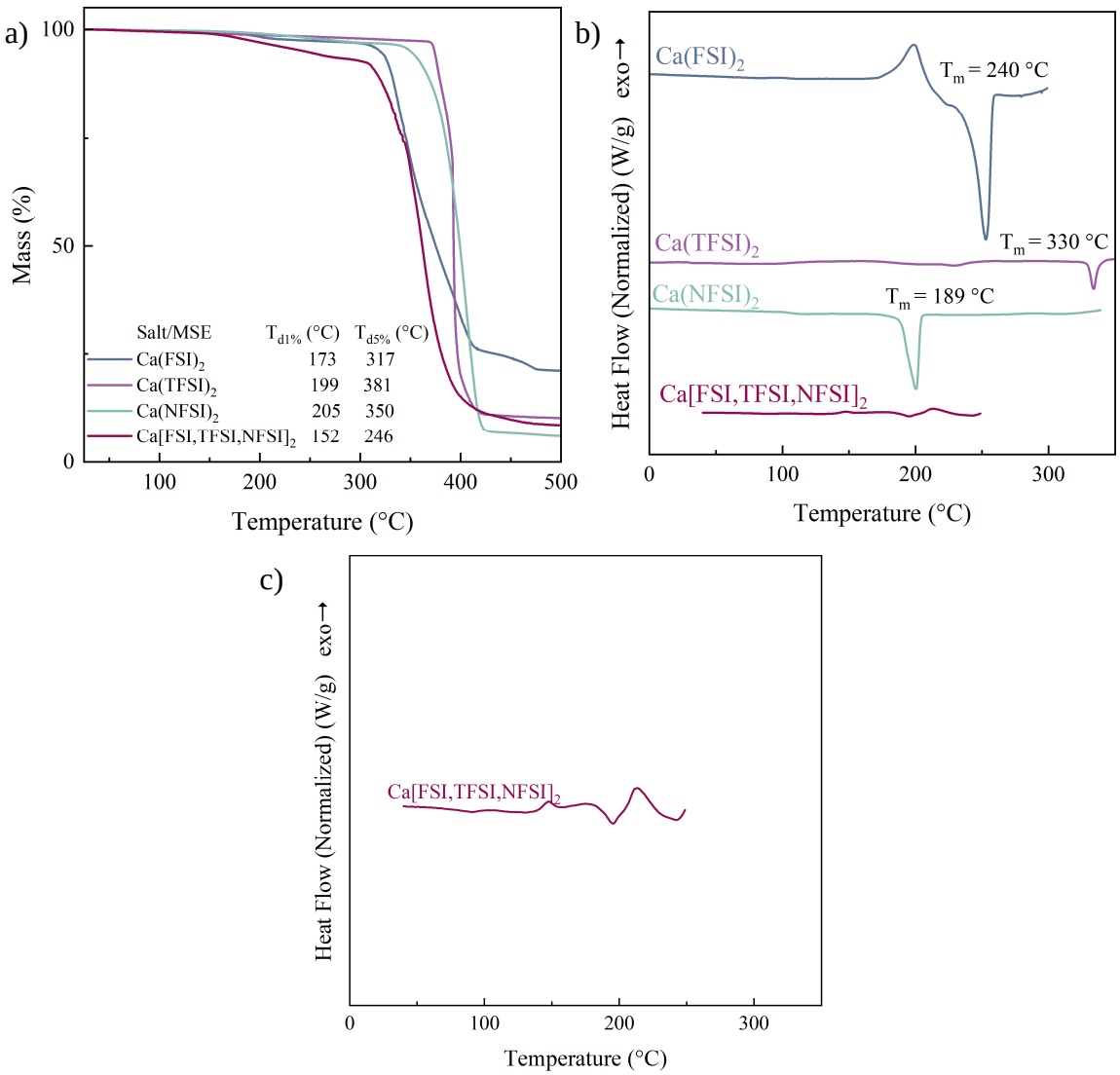

Figure 5.1. Graphs of single Ca-salt and the MSE Ca[FSI,TFSI,NFSI]$_2$ where a) show TGA traces of the decomposition behaviour, b) show DSC traces of the melting behaviour and c) close-up of Ca[FSI,TFSI,NFSI]$_2$.

5.2 Multi-cationic TFSI-based MSEs

With the prospect of studying the effect of high entropy, and inspired by the community of HEA, creating systems with 5 or more salts [66], were wished for. By first creating a quintenary system, and then removing one salt at a time, effectively creating four quaternary systems, the effect of one single salt's contribution to the system could be studied. The choice fell on the relatively low melting salts of [M]FSI (M = Ca, Li, Na, K, Cs). However, as no CsFSI was commercially available for purchase, the analogous TFSI-salts were picked as an alternative, and thus, the system of [Ca,Li,Na,K,Cs]TFSI was created.

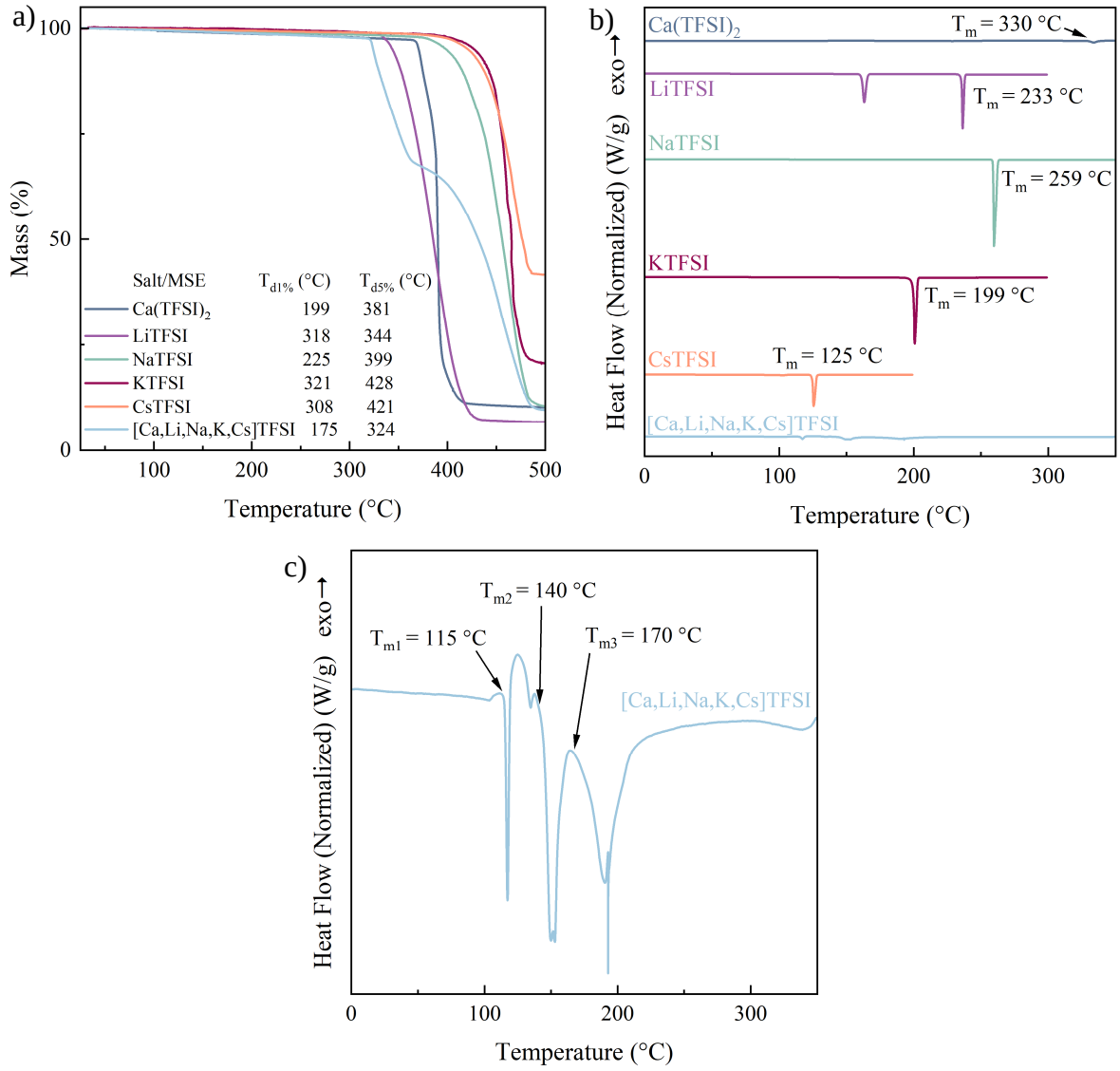

Salt/MSE	$T_{d1\%}$ (°C)	$T_{d5\%}$ (°C)
$Ca(TFSI)_2$	199	381
LiTFSI	318	344
NaTFSI	225	399
KTFSI	321	428
CsTFSI	308	421
[Ca,Li,Na,K,Cs]TFSI	175	324

Figure 5.2. Graphs of single TFSI-salt and the MSE [Ca,Li,Na,K,Cs]TFSI where a) show TGA traces of the decomposition behaviour, b) show DSC traces of the melting behaviour and c) show a close-up of [Ca,Li,Na,K,Cs]TFSI.

In Figure 5.2, TGA and DSC traces of the single salts and the MSE [Ca,Li,Na,K,Cs]TFSI can be seen. The single TFSI-salts have a large spread in Td, particularly for $T_{d5\%}$ which ranges from 344 °C for LiTFSI to 428 °C for KFSI. [Ca,Li,Na,K,Cs]TFSI has a $T_{d5\%}$ of 324 °C, which is lower than for any of the single salts, and additionally, it has a stepwise decomposition. Regarding the T_m, it ranges from 125-235 °C for the alkali metal salt, which is expected from literature [52]. $Ca(TFSI)_2$, which can be seen in Figure 5.2, but is more easily seen in Figure 5.1, has a T_m of 330 °C. [Ca,Li,Na,K,Cs]TFSI show several peaks, the first of them (T_{m1}) at 115 °C, followed by peaks at 140 °C and 170 °C.

It has been suggested that systems, particularly those of metals, that show two eutectic peaks have produced cocrystals [76]. The corresponding concept in MSEs would be that of the formation of complex ions, which are prone when mixing ions with different charge structures.

This effect is further enhanced when large cations like Cs^+ are combined with multivalent cations [75]. The several melting peaks shown for [Ca,Li,Na,K,Cs]TFSI in Figure 5.2, are not enough proof of the existence of complex ions in the system. However, combined with the stepwise decomposition seen in TGA, it is enough to conclude that this system does not form a homogenous mixture. With the higher melting temperatures of TFSI-based salts, compared to that of FSI-based salts, and with no added benefit gained from the addition of a fifth salt, no further quaternary systems based on TFSI were created.

5.3 Multi-cationic FSI-based MSEs

Here, one quaternary and three ternary multi-cationic MSEs with FSI as the single anion is presented. All combinations contain the divalent Ca^{2+} cation together with the monovalent Li^+, Na^+ and K^+ cations, making these mixture charges asymmetric. To emphasise each salt's contribution to the MSEs, the properties of the single salts are included as well. Additionally, one ternary and three binary MSEs without Ca^{2+}, were made as references to highlight the effect of Ca^{2+}.

5.3.1 Thermal properties

As can be seen in Figure 5.3, the single FSI-salts have their $T_{d1\%}$ and $T_{d5\%}$ at around 170-200 °C and 300-320 °C, respectively. Apart from LiFSI which decomposes earlier at 208 °C. This agrees well with literature for the alkali metal salts [57]. There is no previously reported literature on T_d for $Ca(FSI)_2$, however, the presented data follow the same trend as the other salts. Decomposition in single salts is decided by the breakdown of the anion, as all these salts contain the same anion, the difference comes down to the cations. Apart from LiFSI, there is no big difference between the other salts.

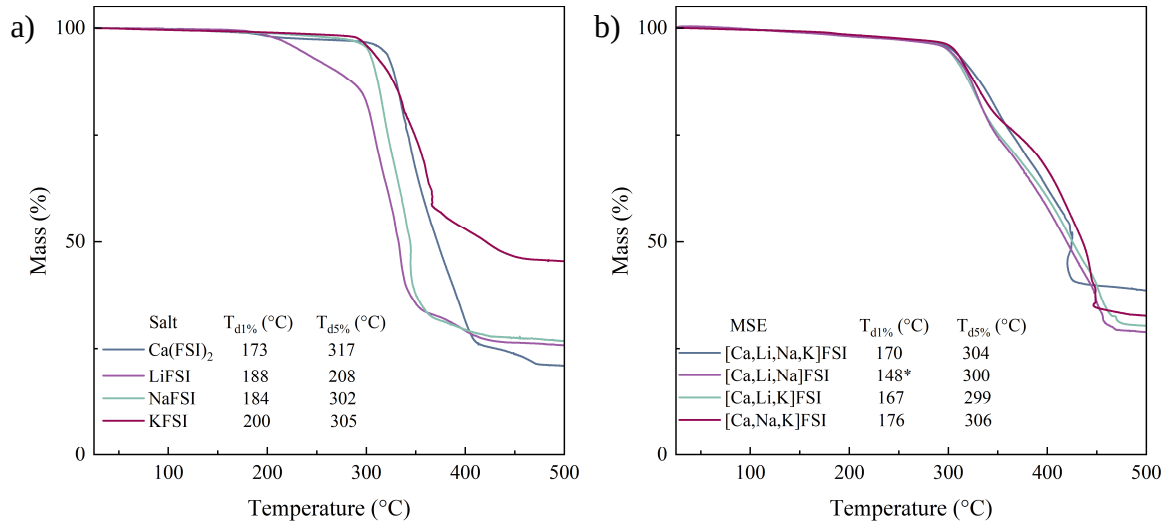

Figure 5.3. TGA traces of a) single salts and b) molten salt electrolytes. The insets highlight the decomposition temperatures.

The MSEs all follow the same trend of decomposing at around 176 °C and 300 °C for $T_{d1\%}$ and $T_{d5\%}$, respectively. The expectation is [Ca,Li,Na]FSI, which appears to decompose already at 148 °C, but this is rather a result of fluctuations in the instrument. As these MSEs are built up of single FSI-salts, it is expected that the weakest bond of the single salt will also be the weakest bond of the MSEs. The MSEs containing LiFSI marginally have the lower $T_{d5\%}$ with the order of highest to lowest corresponding well with the molar fraction of LiFSI in each MSE. Consequently, the only MSE without LiFSI – [Ca,Na,K]FSI – is also the system with the highest $T_{d5\%}$. The significantly lower $T_{d5\%}$ of LIFSI does not appear to affect the MSEs to the extent that perhaps would be expected, as such it is tentatively suggested that the increased entropy of the system might have had somewhat of a stabilizing effect.

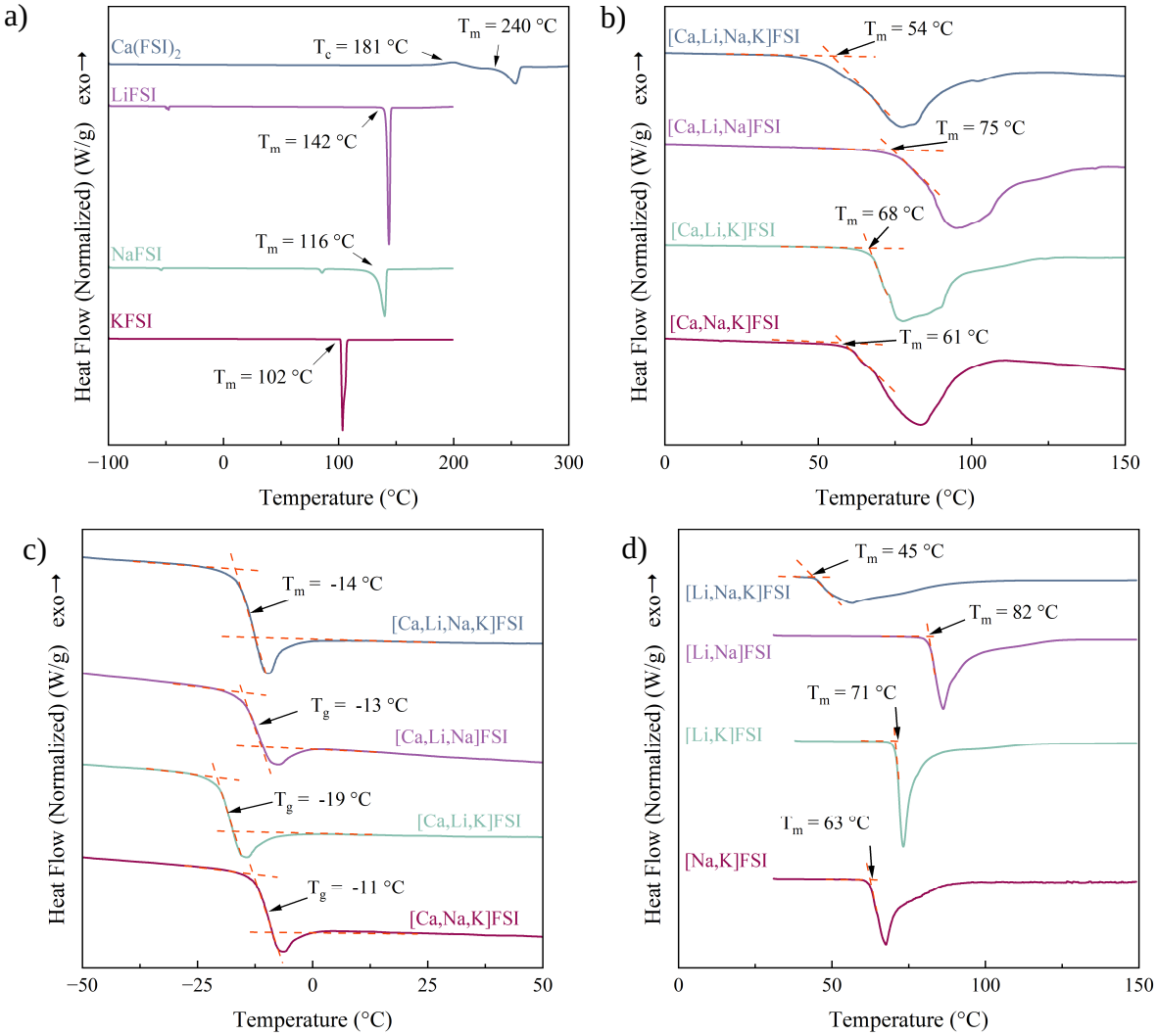

Figure 5.4. DSC traces showing a) melting of single FSI-salts, b) melting of MSEs containing Ca^{2+}, c) glass transitions of MSEs containing Ca^{2+} and d) melting of MSEs without Ca^{2+}.

For the single FSI-salts (Figure 5.4 a) the T_m for LiFSI, NaFSI and KFSI all lay between 100-140 °C, which agrees well with the literature [57]. $Ca(FSI)_2$ first appears to crystalize at 181 °C, before the onset of melting at 240 °C. The melting behaviour of salts largely depends on the size of the cations and anions. FSI which is large and has a delocalized negative charge has

compared to more simple anions like Cl^-, F^- and NO_3^-, a much lower T_m for its analogous cations. The cation contribution can be seen by the fact that the biggest cation (K^+) also has the lowest T_m. Ca^{2+} which is relatively small, but still roughly the same size as Na^+, and bigger than Li^+, has a much higher T_m. Multivalent cations like Ca^{2+}, have larger columbic attractions, which makes them more robust, and consequently, the T_m is pushed higher.

The T_m of the MSEs lay between 60-75 °C for the ternary mixtures and at 54 °C for the quaternary mixtures, which is all far lower than the single salts. However, it is important to note that these melting points are a result of the initial heating of crystalline powder. As the mixtures are cooled down, they do not go through crystallization but rather a glass. Still, these lowered melting temperatures are achieved by increased ΔS_{mix}, reducing the ΔG_{mix}. Hence, the higher entropy of the quaternary systems results in the lowest melting temperature. Furthermore, the disorder that is created in the systems by using different-sized cations can also be seen, as the system with the smallest cation size difference, [Ca,Li,Na]FSI, is also the system with the highest T_m.

The T_m of the MSEs with Ca^{2+} agrees very well with the literature of eutectic MSEs without Ca^{2+} [57], which begs to differ if Ca^{2+} truly is part of the eutectic solution. Complementary tests of equimolar MSEs without Ca^{2+} were created, which showed slightly higher T_m (Figure 5.4) than previously reported. This indicates that Ca^{2+} is part of the eutectic solution of the original MSEs. Furthermore, by comparing the melting peaks, the addition of Ca^{2+} makes the ΔH_{mix} less endothermic (Table 5.1), which is a consequence of these systems' charge asymmetry [75]. By looking only at the systems containing Ca^{2+}, the lowest ΔH_{mix} primarily depends on the large polarization power of the small Li^+ paired with Ca^{2+}. Only secondarily does ΔH_{mix} depend on the cation size difference of the whole system [75], which is the most disrupted by the large K^+. Hence, the system without Li^+ has the largest ΔH_{mix}.

Table 5.1. Comparison between the enthalpy of mixing of systems with and without $Ca(FSI)_2$.

	ΔH_{mix} (kJ/mol)	
System	with Ca	without Ca
[Li,Na,K]FSI	13	17
[Li,Na]FSI	13	16
[Li,K]FSI	12	19
[Na,K]FSI	17	16

As these electrolytes are to be operating in ambient temperature battery cells, an isothermal TGA test was done (Figure 5.5) at 100 °C for 12 h followed by 120 °C at 12 h (purple line). As can be seen, the sample mass loss (blue line) is almost neglectable, as only 1% of mass loss is recorded after 13 h (1 h of 120 °C), and 5% or even 2% of mass loss is never reached during the test time (24 h).

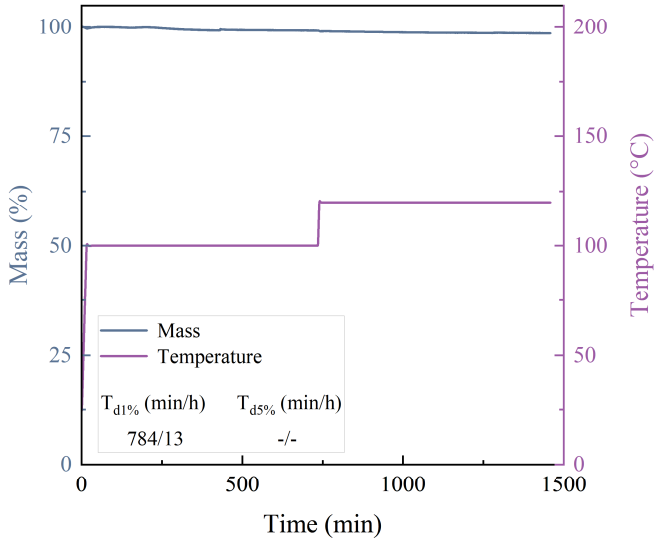

Figure 5.5. Isothermal TGA trace of the MSE [Ca,Li,Na,K]FSI.

5.3.2 Local structure

The local structure of the MSEs has been studied further by Raman spectroscopy. Of particular interest for salts based on FSI, is the 'breathing mode' in the spectral range between 700-800 cm^{-1} (Figure 5.6). The 'breathing mode' of an anion occurs when the bond between two atoms oscillates, which causes the surrounding atoms and bonds to have a responding movement – as a result, all atoms of the ion undergo collective vibration. The simultaneous movement in the ion results in difficulties in assigning the band(s) at this location to just one mode. However, for LiFSI the band at 773 cm^{-1} has been assigned to the symmetric stretching of the S-N-S bonds (ν_sSNS) [83]. As the S-N-S bonds are the physically closest to the cation their movement will also be affected by the cations' size and charge structure. For single salts based on the same anion, the bands are expected to be the same, however, the band frequency is expected to shift in a decreasing manner as the polarizing power of the cations decreases [84].

NaFSI shows one band at 753 cm^{-1} which has been assigned as a combination of scissoring of the SO_2 bonds ($\delta_{sci}SO_2$), stretching of the S-F bond (νSF) and scissoring of the S-N-S bonds (δ_{sci}SNS) [85]. KFSI, which contains the larger K^+ cation, has a different crystal structure compared to the other salts [85], and has three bands in the same region. The first one at 727 cm^{-1} has been assigned as $\delta_{sci}SO_2$ and νSF, while the following two bands at 749 and 768 cm^{-1}, are assigned as $\delta_{sci}SO_2$, νSF and δ_{sci}SNS [85]. The band of $Ca(FSI)_2$ at 772 cm^{-1} has previously not been reported but is here carefully assigned as ν_sSNS. $Ca(FSI)_2$ also have an additional band at 795 cm^{-1}, however, as this band differ from the other salts, it is here left unassigned. The bands of the breathing modes in this spectral range do shift according to polarization power, as expected, apart from the band in $Ca(FSI)_2$. Despite Ca^{2+} having larger polarization power than Li^+ [86], the band appear shifted marginally lower.

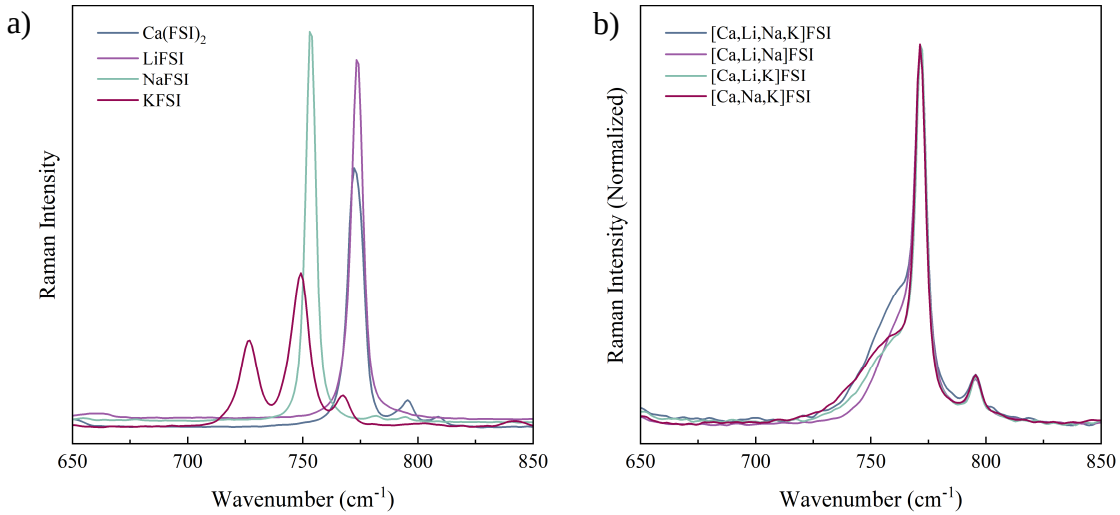

Figure 5.6. Raman spectra of a) single salts and b) MSEs in the spectral range between 650-850 cm^{-1}.

The MSEs all have one strong band at 772 cm^{-1} followed by the same less intense band at 795 cm^{-1} (Figure 5.6), an indication of $Ca(FSI)_2$ influence that has bands at the same position. Typically, when single salts of the same anion-spices are combined into multi-cationic mixtures of molten salts, the Raman spectra are expected to be simply additive, where the cation fraction of each salt corresponds to the overall shift of the combined salt spectra [84]. However, as these MSEs are charge asymmetric, it is not certain that the enthalpy of mixing is ideal and as such the overall spectra cannot be guaranteed to be additive. The clear band at 772 cm^{-1} also have a 'shoulder' connection to it. Broad bands and shoulders are expected of glasses and materials with high entropy [87], due to their amorphous nature. As these MSEs are both glass-forming and have higher entropy, the shoulder is due to amorphous contributions.

5.3.3 Entropy effect

To further see the effect of increased entropy, the stability of the structures was studied. This was done by naturally ageing the MSEs, including the addition of [Li,Na,K]FSI as a reference, inside an argon-filled glovebox for a week. By comparing the spectra of the "aged" MSEs with the spectra of the "as cast" ones (Figure 5.7), it shows that the aged ternary MSEs have lost the 'shoulder' which could be seen before. However, the spectra of the quaternary system have in the same time frame stayed mostly the same. It is not until [Ca,Li,Na]FSI is aged further (> 2 weeks), that it loses the shoulder as well.

The disappearance of the shoulder, and particularly the appearance by the two additional bands at 727 cm^{-1} and 749 cm^{-1}, of all spectrums except that of [Ca,Li,Na]FSI, indicates that it is KFSI that has partially (re-) crystallised/micro-separate from the remaining salts. K^+ is the cation with the lowest polarizing power compared to Ca^{2+}, Li^+ and Na^+, hence, the mobility of K^+ is the greatest out of all the cations. This indicates that the structures of the MSEs are metastable. [Ca,Li,Na]FSI which keeps its amorphous structure for longer, is thus, more stable. The only system not containing Ca^{2+}, [Li,Na,K]FSI, see the same micro-separation of KFSI as the systems with Ca^{2+}. Therefore, it can be concluded that the metastability is not an effect of the

divalent Ca^{2+}, but rather the stabilising effects seen in [Ca,Li,Na,K]FSI is at least partially attributed to the high entropy effect, which has lowered the free energy of the system.

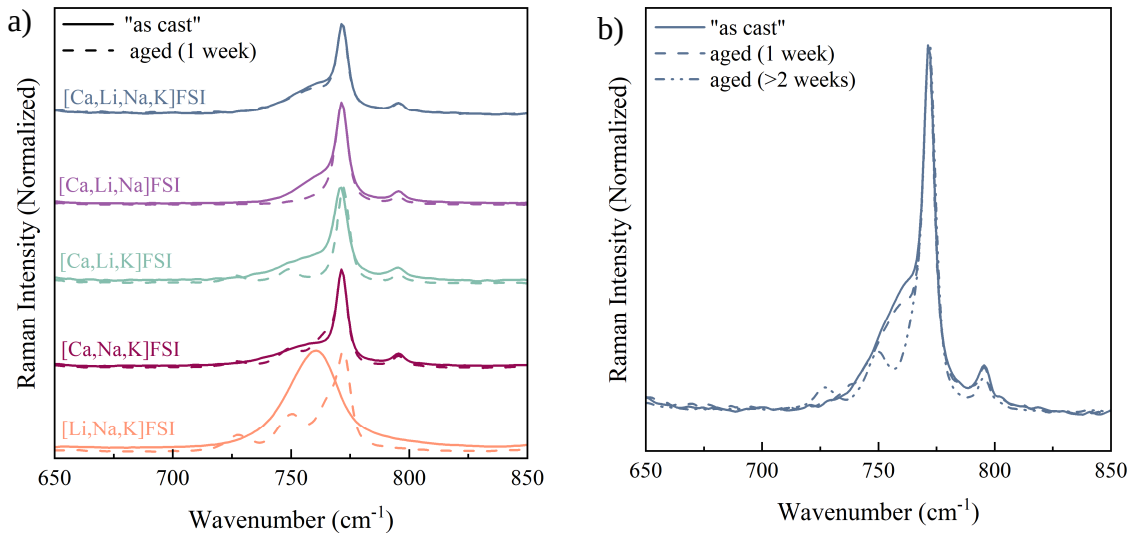

Figure 5.7. Raman spectra of "as cast" and aged MSEs, there a) show all quaternary and ternary systems, and b) show only [Ca,Li,Na,K]FSI.

5.4 Solubility of SEI components

The desire for higher energy density has meant that electrolytes are pushed above their limit [16], thus, the electrolyte decomposes, creating a new phase at the electrode surface, the SEI [18], [21]. Importantly, the SEI must be both stable and conductive to ions, which has been done successfully in LIBs [31]. In new battery technologies, such as Na^+-based ones, the species are more soluble, risking re-dissolving into the electrolyte [79], while in technologies based on multivalent ions like Mg^{2+} and Ca^{2+}, the phases created are often isolating to ions, therefore, blocking charge transfer [6]. The nature and the stability of the SEI layer at the anode are, therefore, fundamentally crucial for both the cycle-life and safety of today's advanced rechargeable batteries [6].

It is then somewhat surprising that relatively few direct efforts targeting solubility properties have been made, given the importance of the SEI for battery functionality. This is possibly connected with experimental difficulties alongside that within the battery community SEI research has almost entirely been devoted to electrode surface studies rather than electrolyte studies [37], [40]. Here, a model was built on experimental data taken from the literature as well complemented with additional experimental values. These were then used for density functional theory (DFT) calculations, used for the subsequent conductor-like screening model for real solvents (COSMO-RS) calculations of the predictive model.

Herein, the experimentally extracted thermal properties are discussed together with solubility data, with a focus on Ca^{2+}. For a deeper analysis of the calculations for the predictive model, please refer to paper II.

5.4.1 Thermal properties

The melting temperature (Tm) and the enthalpy of fusion (ΔH_{fus}), where needed as input to the COSMO-RS calculations. While most of the data was taken from the literature [88], complementary tests were done for LiC_2H_5O, NaC_2H_5O and NaHCOO. As these salts are highly pyrophoric with low flash points, TGA analysis was first performed to understand the decomposition temperature which was needed as a safety limit for the following DSC analysis. Early DSC results showed no traces of the melting peaks. The salts were, therefore, tested above their decomposition temperatures, in pans with pinholes to release any gases formed during the experiment.

In Figure 5.8, the TGA traces of the three salts can be seen that LiC_2H_5O and NaC_2H_5O, which both have the same anion, start to decompose at around 70 °C. This is followed by a stepper decomposition at 164 °C and 188 °C, for Li and Na, respectively. NaHCOO is more stable and has a $T_{1\%}$ of 189 °C and $T_{d5\%}$ of 371 °C. The DSC traces show that LiC_2H_5O only has a small endothermic peak with an onset at 195 °C. NaC_2H_5O and NaHCOO, have sharp peaks which have onsets at 320 °C and 259 °C, respectively.

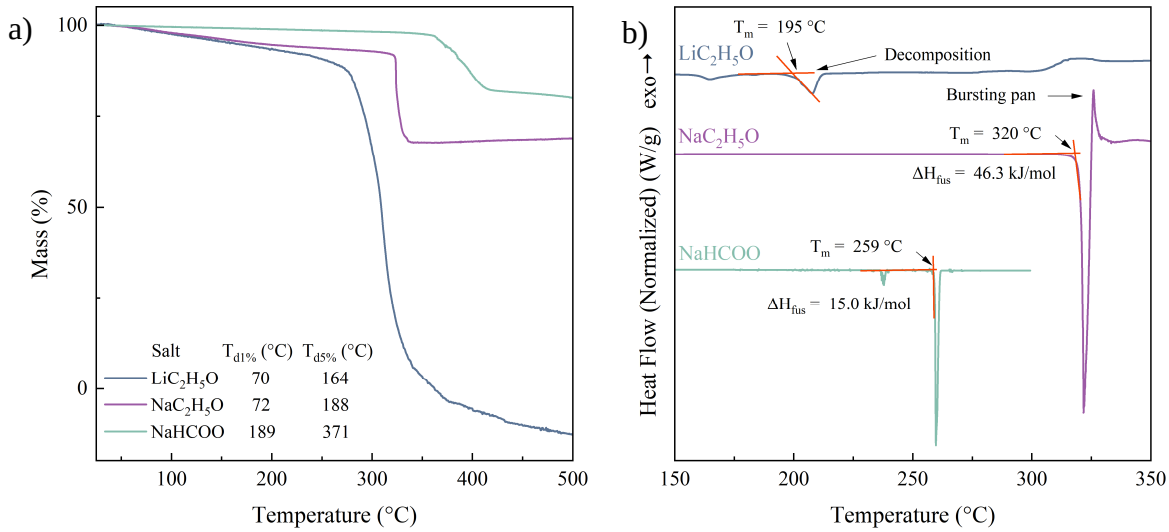

Figure 5.8. SEI-species/salts where a) TGA traces of the decomposition behaviour and b) DSC traces of the melting behaviour and the enthalpy of fusion.

As the salts already have started to decompose before melting, there is a need to study the endothermic peaks in relation to the decomposition temperatures. As such, the decomposition and the onset of the endothermic DSC peak, both happen around 190 °C for LiC_2H_5O, which suggests that the peak is not due to melting but rather decomposition. Therefore, should the corresponding area under the baseline not be assumed to be ΔH_{fus}. The other two salts, NaC_2H_5O and NaHCOO, both exhibit peaks further away from their decomposition temperature, and have sharp peaks which are more typical for the melting of pure salt. Therefore, the only accurate data which can be used for the COSMO-RS model, are those of NaC_2H_5O and NaHCOO. However, NaC_2H_5O reacts with water, creating NaOH, which means that there is no real solubility data for NaC_2H_5O, consequently, only NaHCOO was used in the actual model.

5.4.2 Solubility of SEI species

By using the experimental and literature data of the T_m and the ΔH_{fus}, using DFT and then COSMO-RS, the solubility of 13 salts could be predicted. In Figure 5.9, the predicted solubility can be seen on the y-axis and the experimental solubility data available from literature can be seen on the x-axis. For good agreement between the predicted data and the experimental data, the salts should be located on the dotted line showing ideality. Overall, there is a very good qualitative agreement for the SEI species of Li^+ and Na^+, while for the multivalent cation-based species, and especially for $CaCO_3$ and $MgCO_3$, there are larger deviations. This is due to the intrinsic problem of COSMO-RS to handle non-ideal solubility behaviour, as well as not considering long-range interactions, as such there is difficulty in predicting divalent cations and anions.

Apart from making predictions regarding solubility of Ca^{2+} and Mg^{2+} salts more difficult, the divalent nature of these cations also makes them much less soluble in water, and other solvents, than their monovalent counterparts. The solvent molecules in liquid electrolytes assist the dissociation of the salt so that the cation and anion are free to be transported independently, however, divalent cations have much stronger Columbic interactions [79], which means that they do not easily dissolve. Consequently, new electrolyte strategies for CaBs and magnesium batteries are urged for.

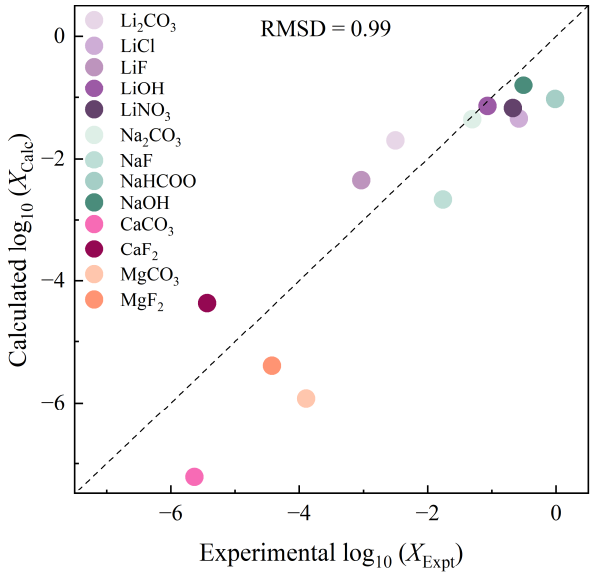

Figure 5.9. Calculated and experimental solubilities in water.

Chapter 6

Summary and outlook

MSEs systems are complex, not the least when combining different cations, anions and their corresponding symmetric or asymmetric charges. As such understanding the underlying thermodynamic properties, such as change in enthalpy and entropy, is the key to creating homogenous low melting systems. Three types of systems have been explored in this thesis, the first, $Ca[FSI,TFSI,NFSI]_2$, which is multi-ionic and does not create a homogenous low melting mixture. All single salts of this system have melting temperatures in the range of 190-330 °C, which cannot be considered low melting but is still so by comparison to the other few commercially available Ca-salts. Consequently, exploring other combinations of multi-anionic Ca^{2+}-based MSEs might not be feasible.

The second system explored was the quintenary multi-cationic TFSI-based system, [Ca,Li,Na,K,Cs]TFSI, which showed several melting peaks. This indicated a non-homogenous melt which also did not reach ambient temperatures. Thus, no quaternary systems were studied further. While a TFSI-based system was not suitable in combination with Ca^{2+}, it does not rule out other quintenary systems with a different anion-base in the future. Not the least by FSI – which undoubtedly has created the most successful systems in this thesis – where there is still hope of eventually purchasing CsFSI as it becomes available. Still, the ternary and quaternary multi-cationic FSI-based MSEs, which were created in this thesis, resulted in homogenous melts at ambient temperatures. Additionally, the quaternary system showed improved stability which is at least partially attributed to the high entropy effect.

The only types of MSEs which have not been explored here are those of mixed cations and anions. These types of systems present a large freedom of which salts can be combined. One such system could be to explore $Ca[FSI,TFSI,NFSI]_2$ – with the addition of an alkali metal salt as a 'softening' agent to the system to reduce the melting temperature and potentially create homogenous mixing. Another option could be to combine LiFTFSI, KFTFSI and CsFTFSI, which all have melting temperatures around 100 °C, with either $Ca(FSI)_2$, $Ca(TFSI)_2$ or $Ca(NFSI)_2$. Three such quintenary systems have in fact been tried but are not included in this thesis as these are still only primary results.

Before diving deeper into systems with such high complexity, it is important to bring back the purpose of creating solvent-free electrolytes in the first place; avoiding passivation layers at the Ca metal anodes in CaBs, created due to organic products in the electrolyte solvent. Therefore, detailed studies of electrochemical properties of the multi-cationic FSI-based MSEs systems for/in CaBs, as well as CaB full cell tests are of utmost importance. For instance, as a battery is charged and discharged the charge carrier concentration in the electrolyte will increase and decrease. Adjustment of the electrolyte composition might, thus, be needed. Furthermore, it is

important to know how the interface and the interphases are affected by the MSEs, and if this strategy is truly successful in creating functional SEI-products, rather than passivation layers.

The solubility of SEI-species containing Li/Na/Ca/Mg was explored in a predictive model by COSMO-RS, which overall showed the qualitatively and the semi-quantitatively calculated solubilities and experimental solubilities correlate well. However, specific deviations did occur and become especially pronounced for Mg and Ca-salts. It highlighted that the solubility of divalent salts is low, and as such, new electrolyte strategies are urged for.

Acknowledgements

First of all, I would like to thank my supervisor Patrik Johansson for allowing me to do my PhD in this excellent group, for great discussions and for pushing me to think more broadly when I'm stuck at organizing the details.

I would also like to thank my assistant supervisor Jonathan Weidow, for his insights, as well as for being there as emotional support and running-advicor.

A big thank you to Ezio Zhangellini, for showing me around the lab, answering all my countless questions and making this division run as smoothly as it does.

A big thank you to previous and current colleagues at the Materials Physics division. It truly feels special to come to work in a place where I feel like I can talk to anyone and be met by a friendly face. You all make lunch and fika so much better.

A special thank you to Josef Rizell, Martina Olsson and Shizhao Xiong, for being the best office mates, for putting up with all my plants and panting, and humouring me when I make powerpoint presentations for suggested changes in the office. It is not the objects in the office, but the people, that makes it the best and warmest place to work in.

I would also like to thank Carolina Cruz Cardona, who since joining the division has been of tremendous help and support, not the least with sorting out this complex world of molten salts.

Thanks to my friends, who uphold some sort of normalcy and give me perspective on what is important in life when I have zoomed in too much on the small stuff.

Finally, to my family, I cannot express just how much your endless support means to me.

Bibliography

[1] J. W. Choi and D. Aurbach, ‘Promise and reality of post-lithium-ion batteries with high energy densities’, *Nature Reviews Materials*, vol. 1. Nature Publishing Group, Mar. 31, 2016. doi: 10.1038/natrevmats.2016.13.

[2] W. Li, B. Song, and A. Manthiram, ‘High-voltage positive electrode materials for lithium-ion batteries’, *Chemical Society Reviews*, vol. 46, no. 10. Royal Society of Chemistry, pp. 3006–3059, May 21, 2017. doi: 10.1039/c6cs00875e.

[3] A. Yoshino, ‘The birth of the lithium-ion battery’, *Angewandte Chemie - International Edition*, vol. 51, no. 24. pp. 5798–5800, Jun. 11, 2012. doi: 10.1002/anie.201105006.

[4] W. Liu, P. Liu, and D. Mitlin, ‘Tutorial review on structure-dendrite growth relations in metal battery anode supports’, *Chemical Society Reviews*, vol. 49, no. 20. Royal Society of Chemistry, pp. 7284–7300, Oct. 21, 2020. doi: 10.1039/d0cs00867b.

[5] A. Ponrouch, J. Bitenc, R. Dominko, N. Lindahl, P. Johansson, and M. R. Palacin, ‘Multivalent rechargeable batteries’, *Energy Storage Mater*, vol. 20, no. February, pp. 253–262, 2019, doi: 10.1016/j.ensm.2019.04.012.

[6] J. D. Forero-Saboya, D. S. Tchitchekova, P. Johansson, M. R. Palacín, and A. Ponrouch, ‘Interfaces and Interphases in Ca and Mg Batteries’, *Adv Mater Interfaces*, vol. 9, no. 8, Mar. 2022, doi: 10.1002/ADMI.202101578.

[7] D. Aurbach, R. Berthelot, A. Ponrouch, M. Salama, and I. Shterenberg, ‘Battery Systems Based on Multivalent Metal and Metal Ions’, in *Prospects for Li-ion Batteries and Emerging Energy ELectrochemical Systems*, L. Monconduit, L. Crouguennec, K. M. Kadish, and R. Guilard, Eds., World Scientific, 2018, pp. 237–318.

[8] D. Aurbach, R. Skaletsky, and Y. Gofer, ‘The Electrochemical Behaviour of Calcium Electrodes in a Few Organic Electrolytes’, *The Electrochemical Society Softbound Proceedings Series*, vol. 138, no. 12, pp. 3536–3545, 1991, doi: 10.1149/1.2085455.

[9] A. Ponrouch, C. Frontera, F. Bardé, and M. R. Palacín, ‘Towards a calcium-based rechargeable battery’, *Nat Mater*, vol. 15, no. 2, pp. 169–172, 2016, doi: 10.1038/nmat4462.

[10] Q. Pang *et al.*, ‘Fast-charging aluminium-chalcogen batteries resistant to dendritic shorting’, *Nature*, vol. 608, pp. 704–711, 2022, doi: 10.1038/s41586-022-04983-9.

[11] D. Linden, T. B. Reddy, and K. W. Beard, ‘Electricity, Electrochemistry, and Batteries: Prologue and Exposition’, in *Linden’s Handbook of Batteries*, Fifth Edition.United States of America: McGraw Hill Education, 2019, pp. 3–21.

[12] B. Scrosati, ‘Lithium batteries: From early stages to the future’, in *Lithium Batteries: Advanced Technologies and Applications*, B. Scrosati, K. M. Abraham, W. van Schalkwijk, and J. Hassoun, Eds., First Edition.Hoboken, New Jersey, USA: John Wiley & Sons, Inc., 2013, pp. 21–38.

[13] J. Y. Hwang, S. T. Myung, and Y. K. Sun, ‘Sodium-ion batteries: Present and future’, *Chemical Society Reviews*, vol. 46, no. 12. Royal Society of Chemistry, pp. 3529–3614, Jun. 21, 2017. doi: 10.1039/c6cs00776g.

[14] J. Bitenc, A. Ponrouch, R. Dominko, P. Johansson, and M. R. Palacin, *Multivalent Charge Carriers*. 2020. doi: 10.1002/9783527610426.bard110020.

[15] H. Gasteiger, K. Krischer, and B. Scrosati, ‘Electrochemical cells: Basics’, in *Lithium Batteries: Advanced Technologies and Applications*, B. Scrosati, K. M. Abraham, W. van Schalkwijk, and J. Hassoun, Eds., First Edition.Hoboken, New Jersey, USA: John Wiley & Sons, Inc., 2013, pp. 1–19.

[16] D. I. Iermakova, R. Dugas, M. R. Palacín, and A. Ponrouch, ‘On the Comparative Stability of Li and Na Metal Anode Interfaces in Conventional Alkyl Carbonate Electrolytes’, *J Electrochem Soc*, vol. 162, no. 13, pp. A7060–A7066, Aug. 2015, doi: 10.1149/2.0091513JES/XML.

[17] T. Thompson and G. E. Blomgren, ‘Battery Component: Section B: Battery Electrolytes’, in *Linden’s Handbook of Batteries*, K. W. Beard, Ed., Fifth Edition.United States of America: McGraw Hill Education, 2019, pp. 61–70.

[18] E. Peled, ‘The Electrochemical Behavior of Alkali and Alkaline Earth Metals in Nonaqueous Battery Systems-The Solid Electrolyte Interphase Model’, *J Electrochem Soc*, vol. 126, no. 12, pp. 2047–2051, 1979, doi: https://doi.org/10.1149/1.2128859.

[19] S. P. Kühn, K. Edström, M. Winter, and I. Cekic-Laskovic, ‘Face to Face at the Cathode Electrolyte Interphase: From Interface Features to Interphase Formation and Dynamics’, *Advanced Materials Interfaces*, vol. 9, no. 8. John Wiley and Sons Inc, Mar. 01, 2022. doi: 10.1002/admi.202102078.

[20] K. Xu, ‘Modern Electrolytes’, in *Electrolytes, Interfaces and Interphases: Fundamentals and Applications in Batteries*, First Edition.Croydon, UK: The Royal Society of Chemistry, 2023, pp. 6–10.

[21] E. Peled and S. Menkin, ‘Review—SEI: Past, Present and Future’, *J Electrochem Soc*, vol. 164, no. 7, pp. A1703–A1719, 2017, doi: 10.1149/2.1441707jes.

[22] A. Ponrouch and M. Rosa Palacín, ‘Post-Li batteries: Promises and challenges’, *Philosophical Transactions of the Royal Society A: Mathematical, Physical and Engineering Sciences*, vol. 377, no. 2152, 2019, doi: 10.1098/rsta.2018.0297.

[23] D. Aurbach *et al.*, ‘Prototype systems for rechargeable magnesium batteries’, *Nature*, vol. 407, pp. 724–727, 2000, [Online]. Available: www.nature.com

[24] R. Dominko, J. Bitenc, R. Berthelot, M. Gauthier, G. Pagot, and V. Di Noto, ‘Magnesium batteries: Current picture and missing pieces of the puzzle’, *J Power Sources*, vol. 478, pp. 378–7753, 2020, doi: 10.1016/j.jpowsour.2020.229027ï.

[25] Z. Zhao-Karger, M. E. Gil Bardaji, O. Fuhr, and M. Fichtner, ‘A new class of non-corrosive, highly efficient electrolytes for rechargeable magnesium batteries’, *J Mater Chem A Mater*, vol. 5, no. 22, pp. 10815–10820, 2017, doi: 10.1039/c7ta02237a.

[26] E. Faegh, B. Ng, D. Hayman, and W. E. Mustain, ‘Practical assessment of the performance of aluminium battery technologies’, *Nat Energy*, vol. 6, pp. 21–29, 2021.

[27] D. Wang, X. Gao, Y. Chen, L. Jin, C. Kuss, and P. G. Bruce, ‘Plating and stripping calcium in an organic electrolyte’, *Nat Mater*, vol. 17, no. 1, pp. 16–20, Jan. 2018, doi: 10.1038/NMAT5036.

[28] Z. Li, O. Fuhr, M. Fichtner, and Z. Zhao-Karger, ‘Towards stable and efficient electrolytes for room-temperature rechargeable calcium batteries’, *Energy Environ. Sci*, vol. 12, p. 3496, 2019, doi: 10.1039/c9ee01699f.

[29] A. Shyamsunder, L. E. Blanc, A. Assoud, and L. F. Nazar, ‘Reversible Calcium Plating and Stripping at Room Temperature Using a Borate Salt’, *ACS Energy Lett*, vol. 4, no. 9, pp. 2271–2276, Sep. 2019, doi: 10.1021/ACSENERGYLETT.9B01550.

[30] M. Li *et al.*, ‘Design strategies for nonaqueous multivalent-ion and monovalent-ion battery anodes’, *Nature Reviews Materials*, vol. 5, no. 4. Nature Research, pp. 276–294, Apr. 01, 2020. doi: 10.1038/s41578-019-0166-4.

[31] K. Xu, ‘Lithium-metal, Lithium-ion and Other Batteries’, in *Electrolytes, Interfaces and Interphases: Fundamentals and Applications in Batteries*, First Edition.Craydon, UK: The Royal Society of Chemistry, 2023, pp. 292–372.

[32] Y. Li, Y. Lu, P. Adelhelm, M. M. Titirici, and Y. S. Hu, ‘Intercalation chemistry of graphite: Alkali metal ions and beyond’, *Chemical Society Reviews*, vol. 48, no. 17. Royal Society of Chemistry, pp. 4655–4687, Sep. 07, 2019. doi: 10.1039/c9cs00162j.

[33] R. J. Gummow, G. Vamvounis, M. B. Kannan, and Y. He, ‘Calcium-Ion Batteries: Current State-of-the-Art and Future Perspectives’, *Advanced Materials*, vol. 30, no. 39. Wiley-VCH Verlag, Sep. 26, 2018. doi: 10.1002/adma.201801702.

[34] X. Deng *et al.*, ‘Anode chemistry in calcium ion batteries: A review’, *Energy Storage Mater*, Dec. 2022, doi: 10.1016/J.ENSM.2022.09.033.

[35] R. D. Shannon, ‘Revised Effective Ionic Radii and Systematic Studies of Interatomie Distances in Halides and Chaleogenides’, 1976.

[36] J. Forero-Saboya, C. Davoisne, R. Dedryvère, I. Yousef, P. Canepa, and A. Ponrouch, ‘Understanding the nature of the passivation layer enabling reversible calcium plating’, *Energy Environ Sci*, vol. 13, no. 10, pp. 3423–3431, Oct. 2020, doi: 10.1039/d0ee02347g.

[37] K. Xu, ‘Electrolytes and interphases in Li-ion batteries and beyond’, *Chem Rev*, vol. 114, no. 23, pp. 11503–11618, 2014, doi: 10.1021/cr500003w.

[38] C. Li *et al.*, ‘An advance review of solid-state battery: Challenges, progress and prospects’, *Sustainable Materials and Technologies*, vol. 29. Elsevier B.V., Sep. 01, 2021. doi: 10.1016/j.susmat.2021.e00297.

[39] Y. Yamada and A. Yamada, ‘Review—Superconcentrated Electrolytes for Lithium Batteries’, *J Electrochem Soc*, vol. 162, no. 14, pp. A2406–A2423, 2015, doi: 10.1149/2.0041514jes.

[40] K. Xu, ‘Nonaqueous liquid electrolytes for lithium-based rechargeable batteries’, *Chem Rev*, vol. 104, no. 10, pp. 4303–4417, 2004, doi: 10.1021/cr030203g.

[41] K. Xu, ‘Ion Transport in Electrolytes’, in *Electrolytes, Interfaces and Interphases: Fundamentals and Applications in Batteries*, First Edition.Craydon, UK: The Royal Society of Chemistry, 2023, pp. 65–130.

[42] K. Xu, ‘Quantification of Ion-Ion Interaction: Debye-Hückel Theory’, in *Electrolytes, Interfaces and Interphases: Fundamentals and Applications in Batteries*, First Edition.Croydon, UK: The Royal Society of Chemistry, 2023, pp. 29–64.

[43] T. Welton, ‘Ionic liquids: a brief history’, *Biophys Rev*, vol. 10, no. 3, pp. 691–706, Jun. 2018, doi: 10.1007/S12551-018-0419-2/SCHEMES/3.

[44] C. A. Angell, Y. Ansari, and Z. Zhao, ‘Ionic Liquids: Past, present and future’, *Faraday Discuss*, vol. 154, pp. 9–27, 2012, doi: 10.1039/c1fd00112d.

[45] J. S. Wilkes, ‘A short history of ionic liquids - From molten salts to neoteric solvents’, *Green Chemistry*, vol. 4, no. 2, pp. 73–80, 2002, doi: 10.1039/b110838g.

[46] S. Sharma, A. S. Ivanov, and C. J. Margulis, ‘A Brief Guide to the Structure of High-Temperature Molten Salts and Key Aspects Making Them Different from Their Low-Temperature Relatives, the Ionic Liquids’, *J. Phys. Chem. B*, vol. 125, p. 43, 2021, doi: 10.1021/acs.jpcb.1c01065.

[47] T. Nohira, ‘Novel electrochemical reactions in molten salts and ionic liquids and their applications’, *Electrochemistry*, vol. 88, no. 6, pp. 477–488, 2020, doi: 10.5796/ELECTROCHEMISTRY.20-00098.

[48] V. Giordani *et al.*, ‘A Molten Salt Lithium−Oxygen Battery’, 2016, doi: 10.1021/jacs.5b11744.

[49] H. Zhou *et al.*, ‘A sodium liquid metal battery based on the multi-cationic electrolyte for grid energy storage’, *Energy Storage Mater*, vol. 50, pp. 572–579, Sep. 2022, doi: 10.1016/j.ensm.2022.05.032.

[50] W. Ding *et al.*, ‘Multi-cationic molten salt electrolyte of high-performance sodium liquid metal battery for grid storage’, *J Power Sources*, vol. 553, p. 232254, Jan. 2023, doi: 10.1016/J.JPOWSOUR.2022.232254.

[51] Y. Song *et al.*, ‘A long-life rechargeable Al ion battery based on molten salts †’, 2017, doi: 10.1039/c6ta09829k.

[52] R. Hagiwara, K. Tamaki, K. Kubota, T. Goto, and T. Nohira, ‘Thermal properties of mixed alkali bis(trifluoromethylsulfonyl)amides’, *J Chem Eng Data*, vol. 53, no. 2, pp. 355–358, 2008, doi: 10.1021/je700368r.

[53] K. Kubota, T. Nohira, T. Goto, and R. Hagiwara, ‘Ternary phase diagrams of alkali bis(trifluoromethylsulfonyl)amides’, *J Chem Eng Data*, vol. 53, no. 9, pp. 2144–2147, Sep. 2008, doi: 10.1021/je800292f.

[54] K. Kubota, K. Tamaki, T. Nohira, T. Goto, and R. Hagiwara, 'Electrochemical properties of alkali bis(trifluoromethylsulfonyl)amides and their eutectic mixtures', *Electrochim Acta*, vol. 55, no. 3, pp. 1113–1119, 2010, doi: 10.1016/j.electacta.2009.09.024.

[55] K. Kubota, T. Nohira, T. Goto, and R. Hagiwara, 'Novel inorganic ionic liquids possessing low melting temperatures and wide electrochemical windows: Binary mixtures of alkali bis(fluorosulfonyl)amides', *Electrochem commun*, vol. 10, no. 12, pp. 1886–1888, 2008, doi: 10.1016/j.elecom.2008.10.001.

[56] K. Kubota, T. Nohira, G. Takuya, and R. Hagiwara, 'Binary and Ternary Mixtures of MFSA (M = Li, K, Cs) as New Inorganic Ionic Liquids', *ECS Trans*, vol. 16, no. 24, pp. 91–98, 2009, doi: 10.1149/1.3109636.

[57] K. Kubota, T. Nohira, and R. Hagiwara, 'Thermal properties of alkali bis(fluorosulfonyl)amides and their binary mixtures', *J Chem Eng Data*, vol. 55, no. 9, pp. 3142–3146, 2010, doi: 10.1021/je9010932.

[58] K. Kubota, T. Nohira, and R. Hagiwara, 'New inorganic ionic liquids possessing low melting temperatures and wide electrochemical windows: Ternary mixtures of alkali bis(fluorosulfonyl)amides', *Electrochim Acta*, vol. 66, pp. 320–324, 2012, doi: 10.1016/j.electacta.2012.01.097.

[59] K. Kubota, T. Nohira, H. Rika, and M. Hajime, 'Thermal Properties of Alkali (Fluorosulfonyl)(trifluoromethylsulfonyl)amides', *Chem Lett*, vol. 39, no. 12, pp. 1303–1304, Nov. 2010, doi: 10.1246/cl.2010.1303.

[60] K. Kubota and H. Matsumoto, 'Melting and crystallization behaviors of alkali metal (fluorosulfonyl) (trifluoromethylsulfonyl)amides', *Chem Lett*, vol. 40, no. 10, pp. 1105–1106, 2011, doi: 10.1246/cl.2011.1105.

[61] K. Kubota and H. Matsumoto, 'Investigation of an intermediate temperature molten lithium salt based on fluorosulfonyl(trifluoromethylsulfonyl)amide as a solvent-free lithium battery electrolyte', *Journal of Physical Chemistry C*, vol. 117, no. 37, pp. 18829–18836, 2013, doi: 10.1021/jp405068q.

[62] K. Kubota and H. Matsumoto, 'Cation Mixtures of Alkali Metal (Fluorosulfonyl)(trifluoromethylsulfonyl)Amide as Electrolytes for Lithium Secondary Battery', *J Electrochem Soc*, vol. 161, no. 6, pp. A902–A907, 2014, doi: 10.1149/2.026406jes.

[63] K. Kubota and H. Matsumoto, 'Lithium Molten Salt Battery at Near Room Temperature Using Low-Melting Alkali Metal Melts', *ECS Trans*, vol. 73, no. 1, pp. 95–100, 2016, doi: 10.1149/07301.0095ecst.

[64] P. W. Atkins, *Physical Chemistry*, Sixth edition. Oxford University Press, 1998.

[65] J. W. Yeh *et al.*, 'Nanostructured high-entropy alloys with multiple principal elements: Novel alloy design concepts and outcomes', *Adv Eng Mater*, vol. 6, no. 5, pp. 299–303, 2004, doi: 10.1002/adem.200300567.

[66] B. S. Murty, J. W. Yeh, S. Ranganathan, and P. P. Bhattacharjee, *High-Entropy Alloys*, Second Edition. Elsevier, 2019.

[67] Y. F. Ye, Q. Wang, J. Lu, C. T. Liu, and Y. Yang, 'High-entropy alloy: challenges and prospects', *Materials Today*, vol. 19, no. 6. Elsevier B.V., pp. 349–362, Jul. 01, 2016. doi: 10.1016/j.mattod.2015.11.026.

[68] C. Oses, C. Toher, and S. Curtarolo, 'High-entropy ceramics', *Nature Reviews Materials*, vol. 5, no. 4. Nature Research, pp. 295–309, Apr. 01, 2020. doi: 10.1038/s41578-019-0170-8.

[69] A. Amiri and R. Shahbazian-Yassar, 'Recent progress of high-entropy materials for energy storage and conversion', *Journal of Materials Chemistry A*, vol. 9, no. 2. Royal Society of Chemistry, pp. 782–823, Jan. 14, 2021. doi: 10.1039/d0ta09578h.

[70] W. Zhang *et al.*, 'Decimal solvent-based high-entropy electrolyte enabling the extended survival temperature of lithium-ion batteries to −130 °C', *CCS Chemistry*, vol. 3, no. 4, pp. 1245–1255, Apr. 2021, doi: 10.31635/CCSCHEM.020.202000341.

[71] S. C. Kim *et al.*, 'High-entropy electrolytes for practical lithium metal batteries', *Nat Energy*, Jul. 2023, doi: 10.1038/s41560-023-01280-1.

[72] Q. Wang *et al.*, 'High entropy liquid electrolytes for lithium batteries', *Nat Commun*, vol. 14, no. 1, Dec. 2023, doi: 10.1038/s41467-023-36075-1.

[73] Q. Wang *et al.*, 'Entropy-Driven Liquid Electrolytes for Lithium Batteries', *Advanced Materials*, vol. 35, no. 17, Apr. 2023, doi: 10.1002/adma.202210677.

[74] S. C. Kim *et al.*, 'Supplementary Information: High-entropy electrolytes for practical lithium metal batteries', *Nat Energy*, 2023.

[75] O. J. Kleppa, 'Thermodynamic properties of molten salt solutions', 1977.

[76] D. Yu, Z. Xue, and T. Mu, 'Eutectics: Formation, properties, and applications', *Chemical Society Reviews*, vol. 50, no. 15. Royal Society of Chemistry, pp. 8596–8638, Aug. 07, 2021. doi: 10.1039/d1cs00404b.

[77] G. J. Janz, 'Physical Properties and Structure of Molten Salts', *J Chem Educ*, vol. 39, no. 2, pp. 59–67, 1962, doi: https://doi.org/10.1021/ed039p59.

[78] K. Xu, 'When an Electrode Operates Beyond Electrolyte Stability Limits: Interphase', in *Electrolytes, Interfaces and Interphases: Fundamentals and Applications in Batteries*, First Edition.Craydon, UK: The Royal Society of Chemistry, 2023, pp. 209–222.

[79] K. Xu, 'Interphases', in *Electrolytes, Interfaces and Interphases: Fundamentals and Applications in Batteries*, First Edition.Craydon, UK: The Royal Society of Chemistry, 2023, pp. 602–713.

[80] G. R. Heal, 'Thermogravimetry and Derivative Thermogravimetry', in *Principles of Thermal Analysis and Calorimetry*, P. J. Haines, Ed., Cambridge CB4 0WF, UK: The Royal Society of Chemistry, 2002, pp. 10–54.

[81] P. G. Laye, 'Differential Thermal Analysis and Differential Scanning Calorimetry', in *Principles of Thermal Analysis and Calorimetry*, P. J. Haines, Ed., Cambridge CB4 0WF, UK: The Royal Society of Chemistry, 2002, pp. 55–93.

[82] D. C. Harris and M. D. Bertolucci, *Symmetry and Spectroscopy: An Introduction to Vibrational and Electronic Spectroscopy*. Mineola, NY, Unated Stated of America: Dover Publication, Inc., 1989.

[83] M. Beran, J. Příhoda, Z. Žák, and M. Černík, 'A new route to the syntheses of alkali metal bis(fluorosulfuryl)imides: Crystal structure of LiN(SO2F)2', *Polyhedron*, vol. 25, no. 6, pp. 1292–1298, Apr. 2006, doi: 10.1016/J.POLY.2005.09.017.

[84] G. J. Janz and D. W. James, 'Raman spectra and ionic interactions in molten nitrates', *J Chem Phys*, vol. 35, no. 2, pp. 739–744, 1961, doi: 10.1063/1.1731994.

[85] K. Matsumoto, T. Oka, T. Nohira, and R. Hagiwara, 'Polymorphism of alkali bis(fluorosulfonyl)amides (M[N(SO2F) 2], M = Na, K, and Cs)', *Inorg Chem*, vol. 52, no. 2, pp. 568–576, Jan. 2013, doi: 10.1021/IC3010486/SUPPL_FILE/IC3010486_SI_002.PDF.

[86] D. S. Tchitchekova *et al.*, ' On the Reliability of Half-Cell Tests for Monovalent (Li + , Na +) and Divalent (Mg 2+ , Ca 2+) Cation Based Batteries ', *J Electrochem Soc*, vol. 164, no. 7, pp. A1384–A1392, 2017, doi: 10.1149/2.0411707jes.

[87] J. W. E. Drewitt, L. Hennet, and D. R. Neuville, 'From Short to Medium Range Order in Glasses and Melts by Diffraction and Raman Spectroscopy', *Rev Mineral Geochem*, vol. 87, no. 1, pp. 55–103, May 2022, doi: 10.2138/rmg.2022.87.02.

[88] W. M. Haynes, 'Section 6: Fluid Properties', in *CRC Handbook of Chemistry and Physics*, 2012, pp. 146–155. [Online]. Available: http://trc.nist.gov